

# Universal scaling behaviour of the transverse polarization for inclusively produced hyperons in hadron-hadron collisions

V.V.Abramov<sup>1</sup>

Experimental Physics Department,  
Institute for High Energy Physics, P.O. Box 35,  
Protvino, 142281 Moscow region, Russia  
<sup>1</sup>E-mail: abramov\_v@mx.ihep.su

## Abstract

Experimental data on the polarization of hyperons, inclusively produced in hadron-hadron collisions, have been analyzed. It is shown that the existing data can be described by a function of transverse momentum ( $p_T$ ) and two scaling variables  $x_{A\pm} = (x_R \pm x_F)/2$ :  $\mathbf{P}_H = A^\alpha F(p_T)[G(x_{A+} - x_2) - \sigma G(x_{A-} + x_2)]$ . The function  $G(x_{A+})$  is proportional to  $\sin[\omega(x_{A+} - x_1)]/\omega$ , which results for some reactions in an oscillation of  $\mathbf{P}_H$  as a function of  $x_F$ . The  $\omega$ , as well as the magnitude and the sign of the hyperon polarization depend on quark composition of hadrons participating in a reaction. The atomic weight dependence of the  $\Lambda$  hyperon polarization is characterized by the parameter  $\alpha \approx -0.16|x_F|$ . There is an analogy between the scaling properties of the hyperon polarization and the analyzing power ( $A_N$ ) in hadron production reactions. This new scaling law allows one to predict hyperon polarization for reactions and kinematic regions, yet unexplored in experiments and to confront these predictions with future experiments and various models.

*Keywords:* Inclusive Reaction; Polarization; Asymmetry; Spin; QCD  
*PACS:* 13.85.Ni; 13.88.+e; 12.38.Qk

# 1 Introduction

The understanding of spin-dependent effects in inclusive hadron production processes in the framework of QCD is still far from being satisfactory, despite significant experimental and theoretical progress over the past few years. In particular, the study of hyperon polarization ( $\mathbf{P}_H$ ) and the analyzing power ( $A_N$ ) could provide invaluable and completely new insight into the field of “spin physics” and, in addition, might also yield a better understanding of the hadronization process.

In this paper we will study the existing data for one measured spin-dependent quantity (transverse hyperon polarization  $\mathbf{P}_H$  in inclusive reactions  $a + b \rightarrow c^\uparrow + X$ ) from an empirical point of view in collisions of unpolarized protons, antiprotons,  $K^\pm$ ,  $\pi^\pm$  or hyperons with protons or nuclei.

Experiments on hyperon production performed during more than two decades since the first polarization observation [1] have shown that the hyperon polarization is significant in a wide range of beam energies. Almost all the existing data (with an equivalent proton momentum on a fixed target from 4 up to 2049 GeV/c) at medium and high energies are used for the analysis.

The study of  $\Lambda$  hyperon polarization in  $pp$  and  $pA$  collisions has been carried out in many experiments and revealed an approximate scaling behaviour as a function of  $x_F$  variable at fixed  $p_T$ , as well as a function of  $p_T$  at fixed  $x_F$  [2]-[13]. Further investigations of the hyperon and proton polarization using different beams and targets have shown its dependence on the hyperon and the beam flavors, as well as on the target atomic weight [14]-[42]. It has to be mentioned that a large value of the hyperon polarization represents a significant problem for the existing strong interaction theory which predicts, in the framework of perturbative Quantum Chromodynamics (pQCD), the vanishing of the polarization at high  $p_T$  and energy [43]. For the review of the hyperon polarization data and the existing models see [44, 45, 46].

Recently a new scaling law has been proposed for a hadron production analyzing power ( $A_N$ ) in reactions

$$a^\uparrow + b \rightarrow c + X$$

where  $a$ ,  $b$  and  $c$  are hadrons, and the hadron  $a$  is transversely polarized [47, 48]. Since the hyperon polarization and the hadron analyzing power

could be closely related [49], it is reasonable to expect that similar scaling properties take place for the inclusive hyperon production in collisions of unpolarized hadron beams with protons or nuclei. According to Ref. [48]  $A_N$  at high energies ( $\geq 40$  GeV) and high transverse momentum  $p_T$  ( $\geq 1$  GeV/c) can be described by a simple function of two variables,  $p_T$  and  $x_A$ :

$$A_N = F(p_T)G(x_A), \quad (1)$$

where

$$x_A = p_c \cdot p_b / p_a \cdot p_b = E_c / E_a. \quad (2)$$

Here,  $p_c$ ,  $p_b$  and  $p_a$  are four-momenta of the produced hadron, the target hadron and the beam hadron, respectively. The energies  $E_c$  (produced hadron) and  $E_a$  (beam hadron) are measured in a reference frame, where a polarized ( $p$  or  $\bar{p}$ ) particle strikes an unpolarized target ( $p$  or  $A$ ) which is at rest. There are also alternative expressions for the scaling variable  $x_A$ , which are close to (2) numerically at the high beam and secondary hadron energies [48]. In particular, neglecting masses in (2), we have in the c.m. frame

$$x_A = (x_F + x_R)/2, \quad (3)$$

where  $x_F = p_z^* / p_{max}^*$  and  $x_R = p^* / p_{max}^*$ . Here  $p^*$ ,  $p_z^*$  and  $p_{max}^*$  is momentum of the produced hadron, its longitudinal component and the maximum possible value of it, respectively, all in the c.m. reference frame. Eqs. (1) and (3) describe  $A_N$  for most of the hadron production reactions almost as well as eqs. (1) and (2) [48]. The only exception is the  $A_N$  for  $\Lambda$  hyperon production in  $p\uparrow p(A)$  collisions, for which the variable (3) is preferable since it gives a smaller  $\chi^2$  ( $\chi^2/N_{DOF} = 24.3/44$  for (3) vs  $39.4/44$  for (2)), where  $N_{DOF}$  is the number of degrees of freedom in a fit. It is interesting that  $\Lambda$  hyperon polarization is also better described by eq. (1) if  $x_A$  is given by (3).

It has to be mentioned that the variable  $x = E_c / E_a$  was used to describe the scaling properties of the secondary hadron ( $\pi, K, \bar{p}, \bar{n}$ ) spectra in the region  $E_c / E_a \geq 0.6 \div 0.7$  [50].

A natural generalization of (3) is given by a linear function of  $x_R$  and  $x_F$  variables with relative weights which could be determined from the data fit:

$$x_{A\pm} = x_R \cdot w_1 \pm x_F \cdot w_2, \quad (4)$$

where  $w_1 + w_2 = 1$ . For  $w_1 = 0.5$  the variable  $x_{A+}$  in (4) is close to  $|x_F|$  in the beam fragmentation region ( $x_F \approx 1$ ) and  $x_{A+} \approx x_T/2$  in the central

region ( $x_F \approx 0$ ). The variable  $x_{A-}$  have similar properties in the backward hemisphere ( $x_F \leq 0$ ). For  $w_1 = 0.5$  variable  $x_{A+}$  is identical to  $x_A$  (eq.(3)).

The hyperon polarization features are different in some respects from the analyzing power features listed in [48]. In particular, we have to take into account that the polarization of hyperons produced in  $pp$  collisions is antisymmetric in  $x_F$  by virtue of rotational invariance [11, 51]:

$$\mathbf{P}_{\mathbf{H}}(x_F, p_T) = -\mathbf{P}_{\mathbf{H}}(-x_F, p_T) \quad (5)$$

From the relation (5) we have also for the hyperon polarization  $\mathbf{P}_{\mathbf{H}}(0, p_T) = 0$  for  $pp$  or other symmetric initial states in contrast to the analyzing power, which could be different from zero even at  $x_F = 0$ , see [48]. The initial state  $p^\dagger p$  is not symmetric with respect to the  $180^\circ$  rotation since one proton is polarized.

From a dimensional analysis alone, the polarization  $\mathbf{P}_{\mathbf{H}}$  admits two types of contributions, which are functions of  $u/s$  and  $t/s$ :

$$\mathbf{P}_{\mathbf{H}} = F(p_T) [G_+(-u/s) - G_-(-t/s)], \quad (6)$$

where  $u$ ,  $t$  and  $s$  are Mandelstam variables:

$$\begin{aligned} s &= (p_a + p_b)^2 \approx +2p_a \cdot p_b, \\ t &= (p_a - p_c)^2 \approx -2p_a \cdot p_c, \\ u &= (p_b - p_c)^2 \approx -2p_b \cdot p_c, \end{aligned} \quad (7)$$

where in the last column the hadron masses are neglected. It is easy to show that at high energies the following approximations are valid:

$$-u/s \approx (x_R + x_F)/2 = x_{A+}, \quad (8)$$

$$-t/s \approx (x_R - x_F)/2 = x_{A-}, \quad (9)$$

where  $x_{A\pm}$  are given by eq. (4) with  $w_1 = 0.5$ . Relations, similar to (8)-(9), have been used in Refs. [52, 53]. Using eqs. (7) - (9) it is easy to show that  $x_{A+} \approx p_c \cdot p_b / p_a \cdot p_b = x_A$ , where  $x_A$  is given by eq. (2).

The expression, which takes into account (5)-(9) and other features of  $\mathbf{P}_{\mathbf{H}}$  is given below:

$$\mathbf{P}_{\mathbf{H}} = A^\alpha F(p_T) [G(x_{A+} - x_2) - \sigma G(x_{A-} + x_2)], \quad (10)$$

where an additional phase  $x_2$  and a signature parameter  $\sigma$  are introduced to take into account a possible violation of (5) for collisions, different from  $pp$  one (for  $pp$  collisions  $x_2 \equiv 0$  and  $\sigma \equiv 1$ ). It is assumed below that  $\sigma = 1$  for  $pA$  collisions, while  $x_2$  could be different from zero. The functions  $F(p_T)$  and  $G(x_{A\pm})$  are determined below from the experimental data.

Exactly the same approach can be used to derive an expression for the  $A_N$ . The difference is that in the last case  $G_+(x) \neq G_-(x)$  in (6), and  $G_+(x_{A+})$  dominates, at least for the  $p^\uparrow p \rightarrow \pi^+ + X$  reaction, as the data fit show, over  $G_-(x_{A-})$ .

For the process  $pp(A) \rightarrow \Lambda + X$  we use an expression

$$F(p_T) = 1 - e^{-\kappa p_T^3} \quad (11)$$

for the  $F(p_T)$ , where  $\kappa$  is a fit parameter and  $p_T$  is measured in GeV/c. The other processes may require a different expression. The exact shape of the  $F(p_T)$  should be measured in future experiments. For the  $G(x_{A\pm})$  we use an expression

$$G(x_{A\pm}) = \frac{c}{2\omega} \cdot \sin[\omega(x_{A\pm} - x_1)], \quad (12)$$

similar to the one, used in [48], which allows one to reproduce such features, as an approximate linear dependence of  $\mathbf{P}_\Lambda$  on the  $x_F$ , and non-linear, sometimes oscillating behaviour of the hyperon polarization for other reactions. The difference of eq. (12) from the corresponding expression in [48] is that the former has an additional factor  $1/(2\omega)$ , that makes parameters  $c$  and  $\omega$  less correlated and reflects the tendency of hyperon polarization magnitude decrease with  $\omega$  rise. The parameters  $w_1$ ,  $c$ ,  $x_1$ ,  $x_2$ ,  $\sigma$  and  $\omega$  are determined from the data.

The  $\Lambda$  polarization data fits indicate that both parameters  $x_1$  and  $x_2$  can depend on  $p_T$  and only at high enough  $p_T \geq 1.5$  GeV/c are compatible with  $p_T$ -independent constant values:

$$x_1 = \eta_0 - \eta_1 e^{-\delta p_T^3}, \quad (13)$$

$$x_2 = (1 - Z/A)(\xi_0 - \xi_1 e^{-\nu p_T^3}), \quad (14)$$

where the target dependent factor  $(1 - Z/A)$  is introduced to insure  $x_2 = 0$  for  $pp$  collisions, as required by relation (5). For a neutron target  $Z/A = 0$ , so the phase  $x_2$  is the only parameter in the above equations which makes the

hyperon polarization for the proton target different from that of the neutron one. This feature of eq. (14) can be used to estimate the difference in the polarization of hyperons produced on the proton and the neutron targets.

The factor  $A^\alpha$  takes into account a possible atomic weight dependence of the hyperon polarization. The  $\alpha$  could be a constant or a function of kinematic variables:

$$\alpha = \alpha_1 |x_F| + \alpha_0, \quad (15)$$

where  $\alpha_0$  and  $\alpha_1$  are fit parameters.

In the beam fragmentation region  $x_R \approx x_F$ , and  $x_{A+} \approx x_F$ , while  $x_{A-} \approx 0$ . So, in this region the dependence of eq. (10) on  $x_F$  is determined, mainly, by the first term  $G(x_{A+} - x_2) \approx G(x_F - x_2)$ . The second term in (10),  $G(x_{A-} + x_2) \approx G(x_2)$  has a weak  $x_F$  dependence. In the target fragmentation region  $x_F$  dependence is determined, mainly, by the  $\sigma G(x_{A-} + x_2) \approx \sigma G(-x_F + x_2)$ .

Eq. (10) for  $\sigma = \pm 1$  can be expressed using (12) in a different way, with the explicit  $x_R$  and  $x_F$  dependences:

$$\mathbf{P}_H = \frac{c}{\omega} A^\alpha \cdot F(p_T) \begin{cases} \cos[\omega(x_R w_1 - x_1)] \sin[\omega(x_F w_2 - x_2)], & \text{if } \sigma = +1; \\ \sin[\omega(x_R w_1 - x_1)] \cos[\omega(x_F w_2 - x_2)], & \text{if } \sigma = -1. \end{cases} \quad (16)$$

Eq. (10) has a more general form, but it coincides with (16) if we choose eq. (12) for  $G(x_{A\pm})$  and set  $\sigma = \pm 1$ . The magnitude of the hyperon polarization is about  $cA^\alpha/\omega$ . It is assumed here that  $F(p_T)$  is equal unity at its maximum.

In case of the analyzing power measurements we have a non-zero contribution to the left-right asymmetry from the polarized hadron (beam or target) only and the feature (5) is not valid. Naively, we may say that the first term,  $G(x_{A+} - x_2)$ , in (10), corresponding to a polarized beam, gives the main contribution to the analyzing power and, as a result, we have eq. (1) for it. For the case of  $\Lambda$  hyperon polarization in the  $pp$  collisions both terms in (10), corresponding to the beam fragmentation and the target fragmentation, have non-zero contributions and cancel each other at  $x_F = 0$ , in accordance to (5).

Relation (5) is not valid in general for collisions of different hadrons, like  $K^-p(A)$  or  $\bar{p}p$  collisions. In these cases we have to use different functions  $G_+(x_{A+})$  and  $G_-(x_{A-})$  of  $x_{A+}$  and  $x_{A-}$ , respectively. In particular, parameter  $x_2$  can be different from zero and  $\sigma$  can be different from unity.

It should be also mentioned, that in the case of a linear function  $G(x_{A\pm})$  and  $\sigma = 1$  the  $x_R$  terms are cancelled in (10). The use of  $\sin(x)$  in (12) makes

$G(x_{A\pm})$  non-linear, that prevents complete cancellation of  $x_R$  terms in (10). A linear case corresponds to the limit  $\omega \rightarrow 0$  in the above equations, while the data fits give for  $pp(A) \rightarrow \Lambda + X$  process  $\omega \approx 3$ , indicating a rather non-linear behaviour of  $G(x_{A\pm})$  at large values of arguments. As we will see in the following sections the  $\omega$  can be expressed for different reactions via a linear combination of terms, which are functions of quantum numbers characterizing the particular reaction (see eq. (21)). Eq. (21) is used below to fix the  $\omega$  in eq. (10) in data fits that allows us to estimate the other parameters with a better accuracy.

It follows from eqs. (10) - (15) that for the hadron-proton collisions the hyperon polarization  $\mathbf{P}_H$  and the analyzing power  $A_N$  obey the Helmholtz equation:

$$\frac{\partial^2 \mathbf{P}_H}{\partial x_{A+}^2} + \frac{\partial^2 \mathbf{P}_H}{\partial x_{A-}^2} + \omega^2 \mathbf{P}_H = 0. \quad (17)$$

Eq. (17) reflects the non-linearity of the  $\mathbf{P}_H$  dependence and its oscillation as a function of scaling variables  $x_{A\pm}$ , which is characterized by the  $\omega$  parameter.

Most of the hyperon production experiments have been performed on nuclear targets, where relation (5) may not be exactly valid. Also, practically all the available data are concentrated in the forward hemisphere. We cannot exclude that future measurements in the backward hemisphere (nuclear target fragmentation region) will show some deviation from (15), which will require a correction of the polarization  $A$ -dependence. An estimate of nuclear effects in the forward hemisphere will be given below on the base of existing data. We assume also for simplicity that the  $\omega$  parameter is the same for the forward and the backward hemispheres and reflects the dynamics of strong interaction.

## 2 Lambda hyperon polarization in $pp$ and $pA$ collisions

The polarization of  $\Lambda$  hyperons ( $\mathbf{P}_\Lambda$ ) in  $pp(A)$  collisions has been measured in many experiments [2]-[13]. The data include proton collisions with protons and different nuclei ( $d, Be, Cu, W$  and  $Pb$ ).

We assume here that for the positive polarization and scattering to the left the hyperon spin is directed along the unit vector  $\vec{n} \equiv \vec{p}_a \times \vec{p}_c / |\vec{p}_a \times \vec{p}_c|$ ,

which is the normal to the production plane. Here,  $\vec{p}_a$  and  $\vec{p}_c$  is a momentum of the beam hadron and that of the produced hyperon, respectively.

The fit parameters for eqs. (10)-(15) are shown in Table 1 for different fit conditions. The fits have been performed for the data [2]-[13].

In the fit # 1 all parameters are free. The use of  $p_T$ -dependent phases  $x_1$  and  $x_2$  in eqs. (13)-(14) improves the fit quality significantly ( $\chi^2/N_{DOF}$  changed from 1.81 to 1.26).

The dependence of phases  $x_1$  and  $x_2$  on  $p_T$  is shown in Fig. 1. As in the case of polarization dependence on  $p_T$  (see Fig. 2) the phases  $x_1$  and  $x_2$  are described well by the terms  $\propto [1 - a \cdot \exp(-b \cdot p_T^3)]$  with a plateau for  $p_T$  above 1-2 GeV/c. The absolute value of  $x_2$  is small in accordance with the approximate validity of the feature (5) for  $pA$  collisions.

The values of  $w_1 = 0.51 \pm 0.05$  and  $\sigma = 1.03 \pm 0.09$  for the fit # 1 are close to the expected ones (0.5 and 1, respectively) with  $\chi^2/N_{DOF} = 1.27$ . So, the fit # 1 supports the choice of scaling variables in the form  $x_{A\pm} = (x_R \pm x_F)/2$  and an approximate rotational asymmetry (5) for the polarization in  $pA$  collisions, though the experimental data exist only in the forward hemisphere. The parameter  $\omega$  in the fit # 1 is equal to  $3.29 \pm 0.38$ . The large value of  $\omega$  excludes the possibility of a linear dependence of polarization on  $x_{A\pm}$  or  $x_F$  variables.

The fit # 2 is made with four parameters fixed ( $\omega = 3.045$ ,  $\sigma = 1$ ,  $w_1 = 0.5$  and  $\alpha_0 = 0$ ) that simplifies eq. (10) and allows one to determine the other parameters with a better accuracy.

An interesting feature of the above fits is that at the first approximation the  $\alpha$  is proportional to  $|x_F|$ . The higher is a hyperon momentum the more its polarization is attenuated by the interactions with a nuclear target. For a heavy nuclear target and a large  $x_F$  we expect a significant attenuation of the polarization in comparison with the  $pp$  collisions case. In particular, for  $x_F = 0.7$  we have  $\alpha = -0.16|x_F| = 0.109$  and the polarization on a Lead target is reduced by a factor  $A^{-0.109} = 0.56$ . On a Beryllium target a corresponding factor is 0.79. A similar order of magnitude for the polarization degradation in complex nuclei can be found in [44], where it is also shown that the polarization degradation is  $p_T$ -independent. The  $p_T$  dependence of  $\mathbf{P}_\Lambda$  is described by the function  $F(p_T)$ , which is sharply rising for  $p_T \leq 1.2$  GeV/c and is practically constant for higher  $p_T$ . The experimental dependence of  $\mathbf{P}_\Lambda$  on  $p_T$  is illustrated in Fig. 2, where the ratio of  $\mathbf{P}_\Lambda$  and  $A^\alpha D(x_{A+}, x_{A-})$



Table 1: Fit parameters of eqs. (10)-(15) for  $\Lambda$  production in  $pp(A)$  collisions. Different fit conditions are explained in the text.

Fit #	1	2
$c$	$-1.22 \pm 0.09$	$-1.22 \pm 0.05$
$\omega$	$3.29 \pm 0.38$	$3.045$
$\sigma$	$1.03 \pm 0.09$	$1.0$
$w_1$	$0.51 \pm 0.05$	$0.5$
$\eta_0$	$0.404 \pm 0.034$	$0.412 \pm 0.017$
$\eta_1$	$0.29 \pm 0.14$	$0.33 \pm 0.14$
$\delta$	$4.6 \pm 1.7$	$4.7 \pm 1.7$
$\xi_0$	$0.077 \pm 0.025$	$0.075 \pm 0.011$
$\xi_1$	$0.218 \pm 0.061$	$0.213 \pm 0.042$
$\nu$	$1.26 \pm 0.23$	$1.24 \pm 0.22$
$\kappa$	$1.89 \pm 0.15$	$1.88 \pm 0.13$
$\alpha_0$	$-0.01 \pm 0.03$	$0.0$
$\alpha_1$	$-0.133 \pm 0.053$	$-0.156 \pm 0.015$
$\chi^2/N_{DOF}$	$325.7/256$	$326.0/260$

is shown, and

$$D(x_{A+}, x_{A-}) = G(x_{A+} - x_2) - \sigma G(x_{A-} + x_2). \quad (18)$$

The ratio is assumed to be a function of  $p_T$  only. An additional cut  $x_F \geq 0.35$  is used for the data shown in Fig. 2 to exclude the points with large fractional errors of the ratio. The data in Fig. 2 show the independence of the ratio on the beam energy,  $x_F$  and the target type, and confirms the scaling behaviour and factorization of the  $p_T$  and  $x_{A\pm}$  dependencies, assumed in (10). New measurements are desirable for  $p_T \geq 1.5$  GeV/c to clarify the  $\mathbf{P}_\Lambda$  and  $F(p_T)$  behaviour at high  $p_T$ .

The dependence of  $\mathbf{P}_\Lambda$  on  $x_F$  is illustrated in Fig. 3, where the most precise polarization data, measured in  $pBe$  collisions at 400 and 800 GeV/c

are shown [10, 11, 12]. The fitting curves reproduce the  $x_F$  dependence, as well as small variations of it with  $p_T$ .

The attenuation of the  $\Lambda$  polarization on nuclear targets and the dependence of the attenuation on  $x_F$  are illustrated in Fig. 4. The measured polarization is divided by  $F(p_T)D(x_{A+}, x_{A-})$  and the corresponding ratio is plotted in Fig. 4 vs  $x_F$ . The data for the  $pp$  [13],  $pBe$  [11], and  $pW$  [3] collisions show a decrease of polarization on  $Be$  and  $W$  targets with  $x_F$  rise in comparison with the proton-proton collisions case. The existing  $\mathbf{P}_\Lambda$  data on medium and heavy nuclear targets are limited in terms of their accuracy and kinematic range. Additional measurements on medium and heavy nuclear targets for positive and negative  $x_F$  are desirable to confirm and clarify the polarization attenuation effects, shown in Fig. 4. It will be interesting also to measure the  $A$ -dependence of the analyzing power  $A_N$  and compare it with that of the hyperon polarization.

The general agreement between the data and the fits # 1 - # 2 can be considered a good one, taking into account statistical and possible systematic errors of the data in different experiments.

We may conclude that  $\Lambda$  polarization reveals a scaling behaviour, when it is presented in a forward hemisphere as a function of two scaling variables  $x_{A\pm}$  (or  $x_R$  and  $x_F$ ) and  $p_T$ .

### 3 Polarization of $\Sigma^{\pm,0}$ and $\Xi^{0,-}$ hyperons in $pp$ and $pA$ collisions

In this section the polarization of  $\Sigma^{\pm,0}$  and  $\Xi^{0,-}$  hyperons in  $pp$  and  $pA$  collisions is analyzed. The corresponding fit parameters are presented in Tables 2 and 3. The fits have been performed using eqs. (10)-(15), and eq.

$$F(p_T) = \begin{cases} p_T/p_T^0, & \text{if } p_T \leq p_T^0; \\ 1, & \text{otherwise;} \end{cases} \quad (19)$$

for the function  $F(p_T)$ , which is found to be more appropriate for an approximation of the polarization dependence on  $p_T$ . For this section and all the following the parameters  $\alpha_0$  and  $w_1$  are fixed ( $\alpha_0 = 0$  and  $w_1 = 0.5$ ).

### 3.1 The $\Sigma^+$ hyperon polarization

The polarization of  $\Sigma^+$  hyperons ( $\mathbf{P}_{\Sigma^+}$ ) in  $pA$  collisions has been measured on a  $Cu$  target at 800 GeV/c [14] and on a  $Cu$  and a  $Be$  targets at 400 GeV [15, 16, 8]. A fit # 1 is made with some parameters fixed due to a limited data statistics. The parameter  $\omega = 1.9 \pm 1.2$  is compatible with the value of  $\omega$  for the case of  $\Lambda$  polarization discussed in the previous section. The fit # 2 is done with the value of  $\omega = 3.045$ , which follows from eq. (21).

The dependence of  $\mathbf{P}_{\Sigma^+}$  on  $p_T$  is illustrated in Fig. 5, where a ratio of  $\mathbf{P}_{\Sigma^+}$  and  $A^\alpha D(x_{A+}, x_{A-})$  is plotted. The curve corresponds to the function  $F(p_T)$  in eq. (19) with  $p_T^0 \approx 1.2$  GeV/c (fit # 2). The function  $F(p_T)$  is well approximated by a linear dependence for  $p_T \leq 1.2$  GeV/c and a plateau for higher  $p_T$  (see Fig. 5), but additional measurements are desirable for higher  $p_T$  and different  $x_F$ .

It was stated in [14] that the  $\Sigma^+$  polarization at 800 GeV/c decreases as a function of  $p_T$  at fixed  $x_F$ . The results of the fit # 2 indicate that such unusual  $p_T$  dependence is probably due to the  $p_T$  dependence of the parameter  $x_2$  in eq. (14). As we can see from eq. (16), the polarization (for  $\sigma = 1$ ) is proportional to  $\sin[\omega(x_F w_2 - x_2)] \approx \sin[3(x_F/2 - x_2)]$ . Since  $x_2 \approx (1 - Z/A)(0.34 - 0.17e^{-0.82p_T^3})$  and  $(1 - Z/A) \approx 0.4$ , the value of  $x_2$  is about 0.09 for  $p_T \leq 0.5$  GeV/c, it starts to grow fast for  $0.5 \leq p_T \leq 1.5$  GeV/c, and has a plateau  $x_2 \approx 0.19$  for higher  $p_T$  values. The value of  $x_F$  in [14] is about 0.46, so  $\mathbf{P}_{\Sigma^+} \propto \sin[3(0.23 - x_2)]$  and decreases with  $p_T$  rise for  $p_T \geq 0.7$  GeV/c. This decrease of  $D(x_{A+}, x_{A-})$  is not compensated by a corresponding increase of the  $F(p_T)$ , that leads to the observed polarization decrease with  $p_T$  rise. If we take  $x_F \geq 0.65$ , such effect as a decrease of polarization with  $p_T$  increasing is not expected. The results of three other  $\Sigma^+$  polarization measurements, which have typical  $x_F \geq 0.52$ , do not reveal a decrease of  $\mathbf{P}_{\Sigma^+}$  with  $p_T$  rise [15, 16, 8].

It was also stated in [14] that an energy dependence of  $\mathbf{P}_{\Sigma^+}$  is observed by comparing the results at 800 GeV/c ( $Cu$  target) [14], at 400 GeV/c ( $Be$  target) [15] and 400 GeV/c ( $Cu$  target) [16]. The observed difference is really due to the different targets ( $Cu$  vs  $Be$ ) and slightly different  $x_F$  values used for this comparison. In the case of comparison of the data on  $Be$  and  $Cu$  targets a strong  $A$ -dependence is the reason of a higher polarization on the  $Be$  target, since  $\alpha = -0.26|x_F|$  (see fit # 1). For the data on  $Cu$  target [16] the corresponding  $x_F \approx 0.52$  and  $\mathbf{P}_{\Sigma^+} = 0.168 \pm 0.017$ , while the 800

Table 2: Fit parameters of eqs. (10)-(19) for  $\Sigma^\pm$  production in  $pp(A)$  collisions.

Fit #	1	2	3	4
$H$	$\Sigma^+$	$\Sigma^+$	$\Sigma^-$	$\Sigma^-$
$c$	$4.4 \pm 1.0$	$4.0 \pm 0.9$	$4.2 \pm 2.5$	$4.2 \pm 4.2$
$\omega$	$1.9 \pm 1.2$	$3.045$	$6.1 \pm 4.0$	$6.090$
$\sigma$	$1.0$	$1.0$	$1.0$	$1.0$
$p_T^0$	$1.21 \pm 0.07$	$1.24 \pm 0.06$	$0.66$	$0.66$
$\eta_0$	$-0.10 \pm 0.31$	$0.107 \pm 0.059$	$0.25$	$0.25 \pm 0.20$
$\eta_1$	$-0.56 \pm 0.79$	$-0.22 \pm 0.62$	$0.0$	$0.0$
$\delta$	$4.7 \pm 7.5$	$5 \pm 19$	$0.0$	$0.0$
$\xi_0$	$0.337 \pm 0.015$	$0.341 \pm 0.013$	$0.307 \pm 0.058$	$0.31 \pm 0.11$
$\xi_1$	$0.172 \pm 0.054$	$0.198 \pm 0.044$	$0.0$	$0.0$
$\nu$	$0.82 \pm 0.28$	$0.98 \pm 0.20$	$0.0$	$0.0$
$\alpha_1$	$-0.26 \pm 0.05$	$-0.24 \pm 0.04$	$-0.26$	$-0.26$
$\chi^2/N_{DOF}$	$33.0/17$	$33.6/18$	$0.06/3$	$0.06/3$

GeV/c data are measured at  $x_F \approx 0.46$  and  $\mathbf{P}_{\Sigma^+} = 0.124 \pm 0.001$ . The data [15] show that the  $\mathbf{P}_{\Sigma^+}$  increases by 0.05 or more, when  $x_F$  is increased from 0.47 to 0.52. So, the expected  $\mathbf{P}_{\Sigma^+}$  for 800 GeV/c and  $x_F = 0.52$  is about  $0.124 + 0.05 = 0.174$ , which is compatible with the measured value  $\mathbf{P}_{\Sigma^+} = 0.168 \pm 0.017$  at 400 GeV/c.

The energy independence of the polarization is confirmed by Fig. 5, where all the data points at two beam energies and two different targets are approximated well by a single function  $F(p_T)$  and are compatible with the scaling law (10), described using  $p_T$  and two scaling variables  $x_{A+}$  and  $x_{A-}$ .

The data fit indicates also that  $\Sigma^+$  polarization decreases on a nuclear target ( $\propto A^{-0.26|x_F|}$ ). The polarization attenuation is more significant at high  $|x_F|$  values, similar to that of for the  $\Lambda$  hyperons.

Table 3: Fit parameters of eqs. (10)-(19) for  $\Xi^{-,0}$  production in  $pp(A)$  collisions.

Fit #	1	2	3	4
$H$	$\Xi^-$	$\Xi^-$	$\Xi^0$	$\Xi^0$
$c$	$-0.81 \pm 0.12$	$-0.81 \pm 0.12$	$-1.37 \pm 0.50$	$-1.37 \pm 0.61$
$\omega$	$5.95 \pm 0.74$	$6.090$	$6.10 \pm 0.92$	$6.090$
$\sigma$	$1.0$	$1.0$	$1.0$	$1.0$
$p_T^0$	$0.4 \pm 0.2$	$0.4 \pm 0.3$	$0.5$	$0.5$
$\eta_0$	$0.29 \pm 0.11$	$0.284 \pm 0.073$	$0.336 \pm 0.023$	$0.336 \pm 0.036$
$\eta_1$	$-0.030 \pm 0.082$	$-0.033 \pm 0.060$	$0.0$	$0.0$
$\delta$	$2 \pm 12$	$2.5 \pm 9.7$	$0.0$	$0.0$
$\xi_0$	$0.00 \pm 0.22$	$0.02 \pm 0.13$	$-0.2$	$-0.20 \pm 0.15$
$\xi_1$	$0.51 \pm 0.12$	$0.50 \pm 0.10$	$0.0$	$0.0$
$\nu$	$3.0 \pm 1.9$	$2.9 \pm 1.5$	$0.0$	$0.0$
$\alpha_1$	$0.03 \pm 0.14$	$0.04 \pm 0.11$	$-0.12$	$-0.12$
$\chi^2/N_{DOF}$	$71.0/46$	$71.0/47$	$5.7/13$	$5.7/13$

We may conclude that the use of two scaling variables ( $x_{A+}$  and  $x_{A-}$ ) in the form of eq. (10) instead of one ( $x_F$ ) resolves the problem of energy dependence of the  $\Sigma^+$  polarization and the problem of its unusual  $p_T$  dependence (see details in [14]), and presents the existing data in the energy independent way.

### 3.2 The $\Sigma^-$ hyperon polarization

The polarization of  $\Sigma^-$  ( $\mathbf{P}_{\Sigma^-}$ ) has been measured at 400 GeV/c in  $pCu$  [17] and  $pBe$  [18] collisions. Since just a few points in  $x_F$  and  $p_T$  has been measured, some of the fit # 3 parameters are fixed, see Table 2. In addition, for the fit # 4 the  $\omega$  parameter was fixed:  $\omega = 6.090$ . According to the fit the  $\mathbf{P}_{\Sigma^-}$  has a maximum near  $x_F \approx 0.67$  with corresponding  $\omega \approx 6$ .

### 3.3 The $\Sigma^0$ hyperon polarization

The polarization of  $\Sigma^0$  ( $\mathbf{P}_{\Sigma^0}$ ) produced in  $pBe$  has been measured at 28.5 GeV/c [5] and at 18.5 GeV/c [19]. Only two data points are available from these two experiments. At 28.5 GeV/c the value of  $\mathbf{P}_{\Sigma^0}$  is  $0.28 \pm 0.13$  ( $x_F = 0.6$ ,  $p_T = 1.01$  GeV/c), and at 18.5 GeV/c it is  $0.23 \pm 0.13$  ( $0 < x_F < 0.75$ ,  $0.5 < p_T < 2$  GeV/c), which is consistent with the  $\Sigma^\pm$  polarization in the same kinematic area.

### 3.4 The $\Xi^-$ hyperon polarization

The polarization of  $\Xi^-$  ( $\mathbf{P}_{\Xi^-}$ ) has been measured at 800 GeV/c in  $pBe$  [20, 21] collisions, and at 400 GeV/c in  $pCu$  [22] and  $pBe$  [23] collisions. The fit # 1 is made with some parameters fixed. The value of parameter  $\omega$  is  $5.95 \pm 0.74$ . In the fit # 2 the  $\omega = 6.090$  is used and the corresponding curve is shown in Fig. 6 for 400 GeV/c  $pBe$  collisions and  $p_T = 1.5$  GeV/c. The data shown in Fig. 6 have an additional cut  $0.8 < p_T < 1.5$  GeV/c to reduce the smearing of the data points due to the  $p_T$  dependence.

The fit # 2 and Fig. 6 data indicate a local maximum in the absolute value of polarization at  $x_F \approx 0.5$ .

The  $A$ -dependence of the  $\mathbf{P}_{\Xi^-}$  is not significant ( $\alpha_1 \approx 0.04 \pm 0.11$ ).

### 3.5 The $\Xi^0$ hyperon polarization

The polarization of  $\Xi^0$  ( $\mathbf{P}_{\Xi^0}$ ) has been measured at 400 GeV/c in  $pBe$  [9] collisions. The data are presented in Fig. 7 vs  $x_F$ . Due to a small number of experimental points some of the fit parameters were fixed near the values which give the best  $\chi^2$ . The fit # 3 is done with the  $\omega$  free and the fit # 4 - with  $\omega = 6.090$ .

The fit # 4 and Fig. 7 data indicate a local maximum in the absolute value of polarization near  $x_F \approx 0.46$ .

The fits # 2 and # 4 indicate a possible decrease in the absolute value of  $\mathbf{P}_{\Xi^0}$  and  $\mathbf{P}_{\Xi^-}$  for  $x_F \geq 0.6 - 0.8$  due to a high value of  $\omega \approx 6$ . This feature makes these reactions different from the  $\Lambda$  production in  $pA$  collisions, where we see a steady increase of polarization with  $x_F$  rise.

An interesting observation follows from the analysis of the scaling properties of hyperon ( $\Lambda$ ,  $\Sigma^\pm$ ,  $\Xi^-$  and  $\Xi^0$ ) polarization in  $pp(A)$  collisions - the

parameter  $\omega$  (“polarization oscillation frequency”) in eqs. (10)-(19), which describes the rate of change of the polarization with  $x_{A\pm}$  increase, is related with the number of sea quarks ( $N_{SEA}$ ), picked up from the sea during a hyperon production:  $\omega \approx 3N_{SEA}$ .

## 4 Polarization of $\Lambda$ , $\Xi^-$ and $\bar{\Lambda}$ hyperons produced in $K^-p$ collisions

In this section we analyze the hyperon polarization data in  $K^-p$  collisions. The corresponding fit parameters are presented in Table 4. Since the initial state ( $K^-p$ ) is not symmetric vs the rotation transformation and there are no measurements on nuclear targets, some modification of eqs. (10)-(19) is introduced. In particular, the parameters  $\alpha_0$ ,  $\alpha_1$  are fixed at zero values,  $w_1 = 0.5$ , and the factor  $(1 - Z/A)$  in eq. (14) is omitted:

$$x_2 = \xi_0 - \xi_1 e^{-\varepsilon p_T^3}. \quad (20)$$

The function  $F(p_T)$  is given by eq. (19). The  $\sigma$  parameter in (10) could be different from unity due to an asymmetric initial state.

### 4.1 The $\Lambda$ polarization in $K^-p$ collisions

The polarization of  $\Lambda$  ( $\mathbf{P}_\Lambda$ ) hyperons in  $K^-p$  collisions has been measured at 176 GeV/c [7], at 32 GeV/c [24], at 14.3 GeV/c [25, 26], and at 10 and 16 GeV/c [27]. The data with lower beam momenta are not used for this analysis due to the energy dependence of the polarization below 9 GeV/c at fixed negative  $x_F$  [24, 25, 26, 28]. The interesting feature of these  $K^-$  beam data is that they include both, the beam and the target fragmentation regions. That feature allows us to estimate the  $\sigma$  parameter in eq. (10) and check that the scaling behaviour is valid for both hemispheres.

Only the data with  $|x_F| \leq 0.90$  are used for this analysis to avoid a large contribution of exclusive channels near the kinematic limits.

The data fits (# 1 and # 2) have been performed with some parameters fixed due to a limited statistics. In the fit # 1 the parameter  $\omega$  is free, and in the fit # 2 its value is fixed at  $\omega = 3.58$ . Both fits have  $\chi^2/N_{DOF}$  about 1.6 and indicate the maximum near  $x_F = 0.7$  and almost  $x_F$ -independent

polarization for the negative  $x_F$  region. The  $\sigma$  parameter is *negative* in contrast to the  $pp$  data.

The  $p_T$  dependence of the  $\mathbf{P}_\Lambda$  is compatible with a linear rise of the  $F(p_T)$  (see eq. (19)) for  $p_T \leq 0.85$  GeV/c.

Table 4: Fit parameters of eqs. (10)-(20) for  $\Lambda$  and  $\Xi^-$  production in  $K^-p$  collisions.

Fit #	1	2	3	4
$H$	$\Lambda$	$\Lambda$	$\Xi^-$	$\Xi^-$
$c$	$4.18 \pm 0.47$	$4.25 \pm 0.37$	$6.0 \pm 2.8$	$6.8 \pm 2.7$
$\omega$	$3.53 \pm 0.22$	$3.58$	$3.04 \pm 0.88$	$3.58$
$\sigma$	$-0.77 \pm 0.12$	$-0.77 \pm 0.11$	$-0.90 \pm 0.67$	$-1.09 \pm 0.51$
$p_T^0$	1.0	1.0	1.0	1.0
$\eta_0$	$0.076 \pm 0.019$	$0.079 \pm 0.016$	$0.127 \pm 0.049$	$0.142 \pm 0.038$
$\eta_1$	$0.81 \pm 0.21$	$0.80 \pm 0.20$	$-0.01 \pm 0.13$	$-0.046 \pm 0.065$
$\delta$	26	26	26	26
$\xi_0$	$0.191 \pm 0.063$	$0.19 \pm 0.06$	$0.06 \pm 0.16$	$0.09 \pm 0.08$
$\xi_1$	$0.18 \pm 0.13$	$0.19 \pm 0.11$	$-0.42 \pm 0.22$	$-0.34 \pm 0.12$
$\nu$	7	7	27	27
$\chi^2/N_{DOF}$	88.8/55	88.9/56	12.9/11	13.3/12

## 4.2 The $\Xi^-$ polarization in $K^-p$ collisions

The polarization of  $\Xi^-$  ( $\mathbf{P}_{\Xi^-}$ ) hyperons in  $K^-p$  has been studied at 5 GeV/c [29] and at 4.2 GeV/c [30]. Since the polarization in [29] is integrated over one of the variables ( $x_F$  or  $p_T$ ), we have to assign mean values for these integrated variables. As estimates of these mean values we take for the analysis  $x_F = 0.6$ , and  $p_T = 0.3$  GeV/c, respectively. Only data with  $|x_F| \leq 0.85$  are used for the analysis to exclude the resonance region, in particular in the extreme



forward region ( $x_F \approx 1$ ) which is dominated by the baryon exchange process  $K^-p \rightarrow \Lambda\pi^0$ . The fit # 3 is made with the  $\omega$  parameter free, and the fit # 4 is made for  $\omega = 3.58$ . As in the case of the  $\Lambda$  polarization the  $\sigma$  parameter is negative, but with a much larger uncertainty.

Additional measurements are desirable for  $p_T \geq 0.5$  GeV/c where polarization could reach high values. Both, the  $x_F$  and the  $p_T$  dependencies of  $P_{\Xi^-}$  are similar to the case of the  $\Lambda$  polarization in  $K^-p$  collisions.

### 4.3 The $\bar{\Lambda}$ polarization in $K^-p$ collisions

The  $\bar{\Lambda}$  polarization in  $K^-p$  collisions has been measured at 32 GeV/c [24]. Since just two  $x_F$  points are available, only the magnitude of polarization is estimated which is about 0.4.

## 5 Hyperon polarization in $K^+p$ collisions

The hyperon polarization data for  $K^+p$  collisions have been analyzed using eqs. (10)- (20). Only the data with  $|x_F| \leq 0.74$  are used for the analysis. The fit parameters are presented in Table 5.

### 5.1 The $\Lambda$ polarization in $K^+p$ collisions

The  $\Lambda$  polarization in  $K^+p$  collisions has been measured at 8.2 and 16 GeV/c [31], at 13 GeV/c [32], and at 32 GeV/c [24]. The fit # 1 is made with the  $\omega$  parameter free, and the fit # 2 - with the  $\omega = 3.58$ . The polarization does not depend on energy and has a maximum near  $x_F = 0.35$ .

### 5.2 The $\bar{\Lambda}$ polarization in $K^+p$ collisions

The  $\bar{\Lambda}$  polarization in  $K^+p$  collisions has been measured at 32 and 70 GeV/c [33], at 8.2 and 16 GeV/c [31], at 32 GeV/c [24], and at 13 GeV/c [32]. The data [33] for 32 and 70 GeV/c are combined for this analysis and an average momentum 50 GeV/c is assigned to it. The fit # 3 and the fit # 4 have been performed with  $\omega$  parameter free and fixed ( $\omega = 5.55$ ), respectively. The fits result in a negative  $\sigma \approx -1$ , similar to the  $K^-p \rightarrow \Lambda$  case. The fits indicate the existence of significant phases  $x_1$  and  $x_2$ , which depend on

$p_T$ . The hyperon polarization observed in this reaction is higher than in any other one.

Table 5: Fit parameters of eqs. (10)-(20) for  $\Lambda$ , and  $\bar{\Lambda}$  production in  $K^+p$  collisions.

Fit #	1	2	3	4
$H$	$\Lambda$	$\Lambda$	$\bar{\Lambda}$	$\bar{\Lambda}$
$c$	$-3.0 \pm 1.9$	$-2.4 \pm 1.3$	$3.4 \pm 1.1$	$3.9 \pm 1.0$
$\omega$	$4.4 \pm 1.5$	$3.58$	$4.4 \pm 1.9$	$5.55$
$\sigma$	$0.30 \pm 0.18$	$0.36 \pm 0.28$	$-1.24 \pm 0.39$	$-1.40 \pm 0.28$
$p_T^0$	$0.4$	$0.4$	$0.4$	$0.4$
$\eta_0$	$-0.19 \pm 0.13$	$-0.21 \pm 0.13$	$0.12 \pm 0.07$	$0.130 \pm 0.049$
$\eta_1$	$0.0$	$0.0$	$0.24 \pm 0.35$	$0.29 \pm 0.30$
$\delta$	$0.0$	$0.0$	$17 \pm 28$	$17 \pm 20$
$\xi_0$	$-0.53 \pm 0.31$	$-0.73 \pm 0.24$	$0.41 \pm 0.22$	$0.42 \pm 0.16$
$\xi_1$	$0.0$	$0.0$	$0.54 \pm 0.32$	$0.53 \pm 0.17$
$\nu$	$0.0$	$0.0$	$5.7 \pm 5.7$	$4.3 \pm 2.7$
$\chi^2/N_{DOF}$	$9.6/12$	$9.8/13$	$12.4/19$	$13.0/20$

## 6 The $\Lambda$ polarization in $\pi^-p$ and $\pi^+p$ collisions

The hyperon polarization data for  $\pi^\pm p$  collisions have been analyzed using eqs. (10)- (20). The fit parameters are presented in Table 6. A cut  $|x_F| \leq 0.74$  is used to reduce exclusive reaction contributions.

## 6.1 The $\Lambda$ polarization in $\pi^-p$ collisions

The  $\Lambda$  polarization in  $\pi^-p$  collisions has been measured at 3.95 GeV/c [34], at 6 GeV/c [35], at 15 GeV/c [36], at 16.1 GeV/c [37] and at 18.5 GeV/c [38]. The fit # 1 is made with the  $\omega$  parameter free and the fit # 2 is performed with the  $\omega = 3.58$ . The polarization is positive in the target fragmentation region and is negative or near zero for positive  $x_F$ .

## 6.2 The $\Lambda$ polarization in $\pi^+p$ collisions

The  $\Lambda$  polarization in  $\pi^+p$  collisions has been measured at 18.5 GeV/c [38]. The fit # 3 is made with the  $\omega$  parameter free and the fit # 4 is made with the  $\omega = 3.58$ .

The polarization magnitude for  $\Lambda$  hyperons produced in  $\pi^\pm p$  collisions is smaller than it is in the  $pp$  collisions.

# 7 Polarization of antihyperons produced using baryon and antibaryon beams

The reactions presented in this section can be considered as exotic ones due to a very unusual behaviour of the corresponding polarization with the rise of scaling variables. This behaviour cannot be predicted by the existing models. Most of the theoretical models predict zero polarization for antihyperon production in  $pp(A)$  collision since they do not have valence quarks common with the beam or target hadrons. The recent experiments have revealed non-zero polarization for  $\bar{\Xi}^+$  [21] and  $\bar{\Sigma}^-$  [14] hyperons. Other antihyperons also indicate non-zero polarizations with small but not negligible magnitudes.

The fit parameters are presented in Table 7. The  $\alpha$  parameter in eq. (10) is set to zero due to a limited statistics and too few used targets.

## 7.1 Polarization of $\bar{\Lambda}$ in $pA$ collisions

The  $\bar{\Lambda}$  polarization have been measured in  $pBe$  collisions at 400 GeV/c [10, 11] and at 800 GeV/c [12].

Although the magnitude of the polarization is very low ( $\simeq 0.02$ ), the fit indicates an oscillation of the polarization as a function of  $x_F$  with good

Table 6: Fit parameters of eqs. (10)-(20) for  $\Lambda$  production in  $\pi^\pm p$  collisions.

Fit #	1	2	3	4
<i>Beam</i>	$\pi^-$	$\pi^-$	$\pi^+$	$\pi^+$
$c$	$-1.8 \pm 0.5$	$-1.7 \pm 0.6$	$-2.2 \pm 2.2$	$-2.5 \pm 2.9$
$\omega$	$4.33 \pm 0.94$	3.58	$5.2 \pm 6.5$	3.58
$\sigma$	1.0	1.0	1.5	1.5
$p_T^0$	1.0	1.0	1.0	1.0
$\eta_0$	$0.564 \pm 0.088$	$0.632 \pm 0.081$	$0.45 \pm 0.46$	$0.64 \pm 0.10$
$\eta_1$	$2.0 \pm 2.1$	$2.5 \pm 1.0$	0.0	0.0
$\delta$	$50 \pm 35$	$49 \pm 16$	0.0	0.0
$\xi_0$	$0.276 \pm 0.044$	$0.264 \pm 0.048$	$-0.14 \pm 0.70$	$-0.35 \pm 0.23$
$\xi_1$	$0.45 \pm 0.47$	$0.50 \pm 0.43$	0.9	0.9
$\nu$	$12 \pm 11$	$13 \pm 11$	1.0	1.0
$\chi^2/N_{DOF}$	20.9/19	21.2/20	0.40/3	0.42/4

$\chi^2/N_{DOF} = 0.81$ . The data fits have been performed for  $\omega$  parameter free (fit # 1) and  $\omega = 22.27$  (fit # 2). Due to a limited statistics and kinematic range of the data, the  $\eta_1$  parameter is fixed at the same value (0.31) as it is for  $\Lambda$  polarization in  $pA$  collisions. As we will see below the large value of  $\omega = 18.5 \pm 5.7$  is typical for such exotic process ( $p \rightarrow \bar{\Lambda}$ ) which corresponds to the  $\Delta B = 2$  exchange, where  $B$  is a baryon number.

## 7.2 Polarization of $\bar{\Xi}^+$ in $pA$ collisions

The  $\bar{\Xi}^+$  polarization have been measured at 800 GeV/c in collisions of a proton beam with a  $Be$  target [21]. The data fit has been performed  $\omega = 65.19$  (fit # 3), which follows from eq. (21). At the same time this value of  $\omega$  is a minimal one which describes the unusual polarization dependence on  $x_F$  with the middle point closer to zero than the other ones. The fit

function indicates that polarization magnitude could be about 0.18. If such an unusual behaviour will be confirmed by future experiments that reaction will be a large challenge to the strong interaction theory. Much more data are desirable since we have only 3 data points for this reaction.

### 7.3 The $\bar{\Lambda}$ polarization in $\bar{p}p$ collisions

The polarization of  $\bar{\Lambda}$  ( $\mathbf{P}_{\bar{\Lambda}}$ ) hyperons in  $\bar{p}p$  collisions has been studied at 176 GeV/c [7]. The fit # 4 is made with  $\omega$  parameter free, and the fit # 5 is made for  $\omega = 14.21$ . The dependence of  $\mathbf{P}_{\bar{\Lambda}}$  on  $x_F$  is shown in Fig. 8 along with fit # 5 predictions for  $p_T = 0.5$  GeV/c and  $p_T = 1.5$  GeV/c, respectively. The predictions are made for 176 GeV/c  $\bar{p}p$  collisions. Both fits indicate local maximums of  $|\mathbf{P}_{\bar{\Lambda}}|$  at  $x_F \approx 0.45$  and at  $x_F \approx 0.65$  and an oscillation of  $\mathbf{P}_{\bar{\Lambda}}$  as a function of  $x_F$  ( $\omega = 16.2 \pm 4.1$ ). An interesting feature of the data is that almost a full period of the oscillations is covered by the data. This observation needs additional conformation in different kinematic regions due to a limited statistics and the kinematic range covered by the data. Additional measurements are desirable to clarify the  $p_T$  dependence of the  $\mathbf{P}_{\bar{\Lambda}}$ .

The large values of  $\omega$  have been found also for  $pp(C) \rightarrow \bar{\Lambda} + X$  and for  $pA \rightarrow \bar{\Xi}^+ + X$  reactions considered above. The dependence of the  $\omega$  parameter on quantum numbers of the hadrons participating in the reaction will be discussed in details below.

### 7.4 Polarization of $\bar{\Sigma}^-$ in $pCu$ collisions

The  $\bar{\Sigma}^-$  polarization has been measured in the  $pCu$  collisions at 800 GeV/c [14]. The fit was not made since only four data points have been measured at fixed  $x_F \approx 0.47$ . The sign of polarization is positive and its magnitude is about  $0.088 \pm 0.011$ .

## 8 Polarization of $\Xi^-$ and $\Omega^-$ in collisions of hyperons and protons with nuclei

In this section we analyze the polarization of  $\Xi^-$  and  $\Omega^-$  hyperons produced by a neutral unpolarized beam containing hyperons and the  $\Xi^-$  polarization

Table 7: Fit parameters of eqs. (10)-(20) for reactions  $pp \rightarrow \bar{\Lambda} + X$ ,  $pp \rightarrow \Xi^+ + X$ , and  $\bar{p}p \rightarrow \bar{\Lambda} + X$ .

Fit #	1	2	3	4	5
<i>Process</i>	$pA \rightarrow \bar{\Lambda}$	$pA \rightarrow \bar{\Lambda}$	$pA \rightarrow \Xi^+$	$\bar{p}A \rightarrow \bar{\Lambda}$	$\bar{p}A \rightarrow \bar{\Lambda}$
$c$	$-0.47 \pm 0.23$	$-0.49 \pm 0.22$	$-16 \pm 12$	$4.5 \pm 2.9$	$3.5 \pm 1.2$
$\omega$	$18.5 \pm 5.7$	$22.27$	$65.19$	$16.2 \pm 4.1$	$14.21$
$\sigma$	$1$	$1$	$1$	$-1$	$-1$
$p_T^0$	$0.34$	$0.34$	$0.4$	$0.6 \pm 0.9$	$0.4 \pm 0.6$
$\eta_0$	$0.185 \pm 0.029$	$0.174 \pm 0.015$	$0.045 \pm 0.007$	$0.071 \pm 0.061$	$0.042 \pm 0.016$
$\eta_1$	$0.31$	$0.31$	$0.0$	$0.0$	$0.0$
$\delta$	$3.7 \pm 1.9$	$4.3 \pm 1.1$	$0.0$	$0.0$	$0.0$
$\xi_0$	$0.309 \pm 0.072$	$0.322 \pm 0.077$	$0.181 \pm 0.007$	$0.294 \pm 0.020$	$0.303 \pm 0.021$
$\xi_1$	$0.07 \pm 0.15$	$0.10 \pm 0.16$	$0.0$	$0.0$	$0.0$
$\nu$	$1.27$	$1.27$	$0.0$	$0.0$	$0.0$
$\chi^2/N_{DOF}$	$12.9/16$	$13.3/17$	$0.00/0$	$0.74/2$	$1.08/3$

produced by  $\Sigma^-$  beam. In addition, the  $\Omega^-$  and the proton polarizations in  $pp(A)$  collisions are analyzed and compared with the hyperon polarization in different reactions. The  $\alpha$  parameter in eq. (10) is set to zero due to a limited number of used targets and statistics.

## 8.1 Polarization of $\Xi^-$ in collisions of $\Lambda$ and $\Xi^0$ with $Be$ target

In this subsection we consider the data on  $\Xi^-$  polarization which have been measured using a neutral unpolarized high energy beam containing  $\Lambda$  and  $\Xi^0$  hyperons [39]. The primary 800 GeV/c proton beam was used to produce a neutral strangeness containing beam, which in its turn interacted with a  $Be$

target. The average momentum of produced  $\Xi^-$  and  $\Omega^-$  hyperons was about 395 GeV/c. This value of momentum was used to estimate the momentum of the neutral beam. It is assumed in this analysis that the ratio ( $R$ ) of the neutral beam momentum to the 800 GeV/c primary momentum is the same as the ratio of  $\Xi^-$  momentum to the neutral beam momentum. These relations give  $R = 0.703$  and the neutral beam momentum about  $R \cdot 800 = 562$  GeV/c. Using this assumption we performed a fit of the data [39]. The fit parameters are presented in Table 8.

The polarization of  $\Xi^-$  was fitted with  $\omega$  parameter free (fit # 1) and with  $\omega = 45.97$  (fit # 2). The  $x_F$  dependence of polarization is shown in Fig. 9 along with the fit # 2 predictions for  $p_T = 0.5$  GeV/c and  $p_T = 1.5$  GeV/c. Though the magnitude of polarization ( $\mathbf{P}_H^{\text{Max}}$ ) is about 0.026 only, a clear  $x_F$  dependence is seen, which is consistent with the oscillation behaviour, predicted by eqs. (10)-(20). The frequency parameter  $\omega = 46.0 \pm 3.7$  is very large and more than a full period of oscillation is seen in Fig. 9.

## 8.2 Polarization of $\Omega^-$ in collisions of $\Lambda$ and $\Xi^0$ with $Be$ target

The  $\Omega^-$  polarization has been measured using unpolarized neutral beam described in the previous subsection [39]. The polarization of  $\Omega^-$  was fitted with  $\omega = 6.090$  (fit # 3). The magnitude of  $\Omega^-$  polarization is about 0.11.

## 8.3 Polarization of $\Omega^-$ in $pBe$ collisions

The  $\Omega^-$  polarization has been measured using 800 GeV/c  $pBe$  collisions for  $0.3 < x_F < 0.7$  and  $0.5 < p_T < 1.3$  GeV/c [40]. The mean value of polarization in this kinematic range is  $-0.01 \pm 0.01$ , but the dependence of it on  $x_F$  clearly indicates its oscillation as a function of  $x_F$  (see Fig. 10). The fit # 4 is performed (see Table 8) with  $\omega$  parameter fixed at 22.27 as is predicted by eq. (21). It has to be mentioned that this large value of  $\omega$  was estimated using the other reactions and at the same time it is quite consistent with the observed  $x_F$  dependence for the  $pBe \rightarrow \Omega + X$  reaction. The magnitude of polarization oscillation is about  $0.032 \pm 0.016$ .

Table 8: Fit parameters of eqs. (10)-(20) for polarization of  $\Xi^-$  and  $\Omega^-$  hyperons in collisions of a neutral unpolarized beam containing  $\Lambda$  and  $\Xi^0$  with  $Be$  target, and the  $\Omega^-$  polarization in  $pBe$  collisions.

Fit #	1	2	3	4
<i>Process</i>	$\Xi^0 \rightarrow \Xi^-$	$\Xi^0 \rightarrow \Xi^-$	$\Lambda \rightarrow \Omega^-$	$p \rightarrow \Omega^-$
$c$	$2.37 \pm 0.44$	$2.37 \pm 0.42$	$2.6 \pm 4.1$	$1.36 \pm 0.69$
$\omega$	$46.0 \pm 3.7$	45.97	6.090	22.27
$\sigma$	-1.0	-1.0	-1.0	1.0
$p_T^0$	1.0	1.0	1.0	0.39
$\eta_0$	$0.151 \pm 0.017$	$0.151 \pm 0.003$	$0.24 \pm 0.10$	$0.064 \pm 0.012$
$\eta_1$	0.0	0.0	0.0	0.0
$\delta$	0.0	0.0	0.0	0.0
$\xi_0$	$0.085 \pm 0.023$	$0.085 \pm 0.002$	$0.14 \pm 0.03$	$0.372 \pm 0.026$
$\xi_1$	0.0	0.0	0.0	0.0
$\nu$	0.0	0.0	0.0	0.0
$\chi^2/N_{DOF}$	13.75/13	13.75/14	0.04/1	0.01/2

#### 8.4 Polarization of $\Xi^-$ in collisions of $\Sigma^-$ with $C(Cu)$ target

The polarization of  $\Xi^-$  has been measured using 330 GeV/c  $\Sigma^-$  beam on Carbon and Copper targets [41]. The polarization of  $\Xi^-$  for a sample, combining the  $C$  and the  $Cu$  target measurements, was fitted with free  $\omega$  parameter (fit # 1) and with  $\omega = 3.045$  (fit # 2). The fit parameters are presented in Table 9. The  $\Xi^-$  polarization is negative and its magnitude is about 0.4.



Table 9: Fit parameters of eqs. (10)-(20) for reactions  $\Sigma^- + C(Cu) \rightarrow \Xi^- + X$  and  $p(C) + p \rightarrow p + X$ .

Fit #	1	2	3	4
<i>Process</i>	$\Sigma^- A \rightarrow \Xi^-$	$\Sigma^- A \rightarrow \Xi^-$	$pA \rightarrow p$	$pA \rightarrow p$
$c$	$-1.53 \pm 0.56$	$-1.51 \pm 0.48$	$0.74 \pm 0.14$	$0.73 \pm 0.10$
$\omega$	$3.3 \pm 3.5$	$3.045$	$6.12 \pm 0.21$	$6.090$
$\sigma$	$0.87 \pm 0.27$	$0.88 \pm 0.23$	$1.0$	$1.0$
$p_T^0$	$1.0$	$1.0$	$0.4$	$0.4$
$\eta_0$	$-0.41 \pm 0.51$	$-0.446 \pm 0.042$	$0.647 \pm 0.014$	$0.648 \pm 0.012$
$\eta_1$	$-0.20 \pm 0.28$	$-0.21 \pm 0.29$	$0.204 \pm 0.045$	$0.205 \pm 0.045$
$\delta$	$4.6$	$4.6$	$1.75$	$1.75$
$\xi_0$	$0.84 \pm 0.71$	$0.88 \pm 0.23$	$1.474 \pm 0.089$	$1.476 \pm 0.090$
$\xi_1$	$0.71 \pm 0.78$	$0.75 \pm 0.34$	$1.75$	$1.75$
$\nu$	$1.3$	$1.3$	$1.75$	$1.75$
$\chi^2/N_{DOF}$	$10.7/17$	$10.7/18$	$35.9/31$	$35.9/32$

## 8.5 The proton polarization in $pp(C)$ collisions

It is interesting to compare the hyperon polarization data with the proton polarization data in  $pp(C)$  collisions. The data have been measured at 100, 200, 300 and 400 GeV/c in collisions of a proton beam with protons and a Carbon target [42]. The data fits have been performed for  $\omega$  parameter free (fit # 3) and  $\omega = 6.090$  (fit # 4). The value of  $\omega = 6.12 \pm 0.21$  is consistent with the corresponding values of  $\omega$  for  $pA \rightarrow \Xi^0(\Xi^-) + X$  reactions, indicating a similar mechanism for the polarization origin. The  $p_T$  dependence of the polarization is mainly due to a significant  $p_T$  dependence of the phases  $x_1$  and  $x_2$ . The data are consistent with the scaling described by eq. (10) with  $F(p_T)$  given by eq. (19).

## 9 Dependence of the hyperon polarization on quantum numbers

There is a very interesting feature of the hyperon polarization, related with the value of the parameter  $\omega$  in eqs. (10)-(14). The results of the data fits indicate (see Table 10) that for the hyperon and antihyperon production in  $pp(A)$ ,  $K^\pm p$ ,  $\pi^\pm p$ ,  $\Sigma^- p$ ,  $\Lambda(\Xi^0)p$ , and  $\bar{p}p$  collisions the  $\omega$  parameter depends on flavors of the projectile, the produced hyperon and the target. It can be expressed for the reaction  $a + b \rightarrow c^\uparrow + X$  using the formula

$$\omega_Q = \sum_{i=1}^{i=5} a_i Q_i, \quad (21)$$

where  $Q_i$  depends on the quark content of hadrons participating in the reaction, and  $a_i$  are fit parameters. In particular,

$$Q_1 = |B_c| [n_q(a\bar{c}) + n_q^{ext}(a\bar{c})], \quad (22)$$

$$Q_2 = B_{a\bar{c}} \Psi(B_a) + 2\delta[n_q(a\bar{c}) - 6]\delta(B_{a\bar{c}}), \quad (23)$$

$$Q_3 = |B_a| |B_c| \{B_{b\bar{c}} + 2\delta[n_q(a\bar{c}) - 6]\delta(B_{b\bar{c}})\}, \quad (24)$$

$$Q_4 = |B_a| \delta(N_s^c - 2) \{\delta[n_q^s(a\bar{c})]\delta[n_q(a\bar{c}) - 2] + \delta[n_q^s(a\bar{c}) - 2]\}, \quad (25)$$

$$Q_5 = \delta(B_a)\delta(B_c), \quad (26)$$

where

$$\Psi(n) = \begin{cases} n, & \text{if } n \neq 0; \\ 1, & \text{otherwise,} \end{cases} \quad (27)$$

and

$$\delta(x) = \begin{cases} 0, & \text{if } x \neq 0; \\ 1, & \text{otherwise.} \end{cases} \quad (28)$$

In the above formulas  $n_q(a\bar{c})$  is the minimal number of quarks in the  $a\bar{c}$  system ( $q\bar{q}$  pairs of the same flavor are cancelled, see quark diagram in Fig. 11). The  $n_q^{ext}(a\bar{c})$  denotes additional (extra) quarks and antiquarks, produced in a process above the minimal level when a higher order quark level diagram is used, as in the case of the process  $p + p \rightarrow p + X$ . In the last mentioned process  $n_q(a\bar{c}) = 0$ , and we assume that the inclusive protons are produced via a single valence quark fragmentation. So, four additional quarks and antiquarks are produced in this process, similar to the case of  $p + p \rightarrow \Xi^- + X$

process, shown in Fig. 11. For all other processes presented in Table 10 the  $n_q(a\bar{c}) > 0$  and  $n_q^{ext}(a\bar{c}) = 0$ . The sum  $N_{spec} = [n_q(a\bar{c}) + n_q^{ext}(a\bar{c})]$  can also be considered as the number of spectator quarks in a process  $a \rightarrow c$ .

We may conclude from the analysis of 22 reactions presented in Table 10 that non-zero number of spectator quark  $N_{spec}$  is always needed (which means quark exchange diagram) to generate a non-zero baryon polarization.

The  $n_q^s(a\bar{c})$  is the net number of  $s$  quarks or antiquarks in the  $a\bar{c}$  system. The  $B_{a\bar{c}}$  and  $B_{b\bar{c}}$  are the baryon numbers of the  $a\bar{c}$  and the  $b\bar{c}$  systems, respectively. The  $B_a$ ,  $B_b$  and  $B_c$  are the corresponding baryon numbers, and  $N_s^c$  is the number of  $s$  quarks in a produced hadron  $c$ .

The value  $n_q(a\bar{c})$  is used in the Constituent Interchange model (CIM) [52] which predicts a cross section at  $p_T = 0$  of the form

$$\frac{Ed^3\sigma}{d^3p}(a \rightarrow c) \sim (1 - x_F)^{2n_q(a\bar{c})-3}. \quad (29)$$

The first term of eq. (21) contributes to the processes  $B+B \rightarrow B+X$ , where  $B$  means baryon ( reactions # 1 - # 5), the second one takes into account the specific properties of the meson induced reactions # 6 - # 12, the third term is important for the antibaryon production, the  $Q_4$  takes into account very high ‘‘oscillation frequency’’ data for the (anti)hyperons, containing *two*  $s$  quarks when the beam hadron has *two* (*zero*)  $s$  quarks (see reactions # 15-16).

The term  $Q_5$  is introduced to take into account the reactions *meson* +  $p(A) \rightarrow \text{meson} + X$ , for which all other terms are zero. The preliminary analysis of analyzing power for these reactions gives  $a_5 \approx 12$  (see also [47]). A detailed study of the meson induced reactions will be made in a separate paper.

The reactions in the Table 10 can be classified according to the set of  $Q_i$  values. The most simple is the case of baryon production in  $pp(A)$  collisions when only the  $Q_1$  term is non-zero and the  $\omega \approx 1.5N_{spec}$  is related with the number of spectator quarks as is illustrated by a quark diagram in Fig. 11. We may suggest that the mean colour field created by the spectator quarks in these reactions is the reason of polarization oscillation as a function of  $x_F$ .

The  $\omega$  values presented in Table 10 were fitted using eq. (21) and the parameters  $a_1 - a_4$  are shown in Table 11. The reactions #11,15,18 and 20-22 were not used in the fit, since they have too few data points.

If the inclusive protons are produced via the single beam quark fragmentation similar to the reaction # 2, then for the number of spectator quarks  $n_q^{ext}(\bar{a}c) = 4$  the predicted value  $\omega_Q = 6.090$  is in a good agreement with the estimated value  $6.12 \pm 0.21$ .

The dependence of the  $\omega$  parameter vs  $\omega_Q$  is shown in Fig. 12 for 15 different reactions, presented in Table 10. The arrows indicate also the predictions of the  $\omega = 0.98$  for the analyzing power in the reactions  $p^\uparrow p \rightarrow \pi(K) + X$ ,  $\omega \approx 12$  in the reactions  $meson + p^\uparrow \rightarrow meson + X$ , and  $\omega \approx 65.2$  for polarization in the reaction  $pp \rightarrow \Xi^+ + X$ .

The line in Fig. 12 shows the result of the fit  $\omega = r \cdot \omega_Q$  with  $r = 1.002 \pm 0.025$  and  $\chi^2/N_{DOF} = 0.38/16$ . This figure confirms a strong correlation of the  $\omega$  parameter with the quantum numbers which characterize the reaction.

The magnitude of hyperon polarization ( $\mathbf{P}_H^{\max}$ ) varies significantly with the hyperon, the projectile and the target flavors and the target atomic weight. The values of  $\mathbf{P}_H^{\max}$  for different reactions were estimated for  $x_F \geq 0$ , where most of the data have been measured, using eqs. (10)-(20) and fit parameters, taken from Tables 1-9. The sign of the  $\mathbf{P}_H^{\max}$  is indicated the same as that for the experimental data if it does not vary in the mentioned above region, and  $\pm$  - otherwise. The results are presented in Table 10 for 22 different reactions.

It is easy to notice from Table 10 that there is a correlation between the value of  $\mathbf{P}_H^{\max}$  and the  $\omega$  parameter for the corresponding reactions. The product of these two values,  $|\mathbf{P}_H^{\max}| \cdot \omega$  varies much less than each value separately.

The  $\sigma$  parameter was found to be consistent with

$$\sigma_Q = \begin{cases} 1, & \text{for } pp(A) \text{ collisions;} \\ -\Phi_Q, & \text{otherwise,} \end{cases} \quad (30)$$

where

$$\Phi_Q = (-1)^{n_c} \Psi(B_c) \Psi(Y_a) \Psi(Y_c) / \Psi(\Delta S_{ac}), \quad (31)$$

where  $Y_a$ ,  $Y_c$ , and  $\Delta S_{ac} = S_a - S_c$  are hypercharges ( $Y = B + S$ ) of  $a$ ,  $c$ , and strangeness change, respectively. The  $n_c$  is the number of quarks with parallel spins in the hadron  $c$ . It is assumed here, in accordance with the  $SU(6)$  quark model [45, 54], that  $n_c = 3$  for the  $\Omega^-$ ,  $n_c = 2$  for the  $\Xi^{0,-}$ ,  $\Sigma^{\pm,0}$ , protons, neutrons, and  $n_c = 1$  for the  $\Lambda$ .

The magnitude  $\mathbf{P}_H^{\max}$  of the polarization can be approximated by

$$P_Q = \frac{\epsilon \Phi_Q}{1 + \Delta\omega(\hat{b})}, \quad (32)$$

where the value of  $\Delta\omega(\hat{b})$  is given by eq.

$$\Delta\omega(\hat{b}) = \sum_{i=1}^{i=5} b_i Q'_i, \quad (33)$$

where

$$Q'_1 = |B_c| n_q^{ext}(a\bar{c}), \quad (34)$$

$$Q'_2 = \delta(B_a)[\Delta S_{ac} - S_a S_c] + 2\delta(S_c + 3)\delta(S_a + 1) \quad (35)$$

$$Q'_3 = |B_a||B_c|\{B_{b\bar{c}}/\Psi[4(n_c - N_s^c) + 1] + \delta[n_q(a\bar{c}) - 6]\delta(B_{b\bar{c}})\}, \quad (36)$$

$$Q'_4 = B_c|B_a|\delta(N_s^c - 2)\{\delta[n_q^s(a\bar{c})]\delta[n_q(a\bar{c}) - 2] + \delta[n_q^s(a\bar{c}) - 2]\}, \quad (37)$$

$$Q'_5 = B_{b\bar{c}}\delta(B_{a\bar{c}}). \quad (38)$$

The  $\epsilon = 0.275 \pm 0.010$  and  $b_i$  are the fit parameters, shown in Table 11.

The fit of  $|\mathbf{P}_H^{\max}|$  using  $|P_Q|$  (the sign of  $\mathbf{P}_H^{\max}$  was not taken into account) was made for the reactions # 1 - # 22. The values of  $P_Q$  are presented in Table 10 with the sign in the region  $x_F > 0$  given by eq. (32).

The magnitude of polarization in the reaction  $pp \rightarrow \Lambda + X$  is  $-\epsilon$ , see eq. (32). For the  $\Xi^-$  and  $\Xi^0$  hyperon production in  $pp$  collisions the magnitude of polarization is  $-\epsilon/2$  due to the factor  $1/\Psi(\Delta S_{ac})$  in eq. (31).

The  $p_T^0$  parameter was found to be consistent with an approximation

$$p_T^0 = k_T^0/[n_q(a\bar{c}) + n_q^{ext}(a\bar{c})], \quad (39)$$

where  $k_T^0 = 2.32 \pm 0.14$  GeV/c.

Eqs. (21) and (32) should have their explanations in the models of strong interaction and ultimately in the QCD, perhaps, in the non-perturbative approach.

The value of parameter  $\omega$  can also be estimated for the processes in which the analyzing power is measured. That requires additional precise measurements in a wide range of  $x_F$  in a kinematic area where the  $x_A$  scaling is fulfilled ( $p_T \geq 1$  GeV/c and/or the beam energy  $\geq 40$  GeV). The reactions with meson beams are of special interest because of a high value of the

$\omega$  parameter and a possibility of “oscillation” of the analyzing power as a function of  $x_F$  (compare Figs. 8- 10 and the preliminary results in [47]).

If we assume that eqs. (10)-(21) are valid also for the analyzing power  $A_N$ , we can make predictions of the  $\omega$  for different reactions.

In particular, we expect  $\omega = 0.98$  for the  $\pi^{\pm,0}$ ,  $K^{\pm,0}$ ,  $\eta$ ,  $K^*(890)$ ,  $\rho$ ,  $\omega$  production in  $pp$  and  $\bar{p}p$  collisions;  $\omega = 3.045$  for the  $\Lambda$  production in  $pp$  collisions;  $\omega = 6.090$  for the proton production in  $pp$  collisions,  $\omega \approx 12$  for  $meson+p^\uparrow \rightarrow meson+X$ , and  $\omega = 22.27$  for the antiproton and  $\bar{\Lambda}$  production in  $pp$  collisions. These predictions include about two tens different reactions and a preliminary analysis confirms these predictions. We may conclude that eq. (21) has a high predictive power which allows one to predict the  $\omega$  parameter for about four tens different spin-dependent processes. It is highly unlikely that the  $\omega$  value in so many different processes is described by the same eq. (21) for accidental reasons. Moreover, within the experimental errors we may fix two out of five parameters:  $a_1 = 3/2$ , and  $a_2 = 1$ .

Eq. (21) also predicts that in some cases a target particle plays a significant role in the dynamics of a hyperon production. This is the case when the baryon number  $B_{b\bar{c}}$  and  $Q_3$  are different from zero.

The scaling behaviour of the  $A_N$  and  $\mathbf{P}_H$  indicates that the corresponding processes take place at the quark or parton level. In case of the discussed above scaling for the analyzing power and for the hyperon polarization such constituents could be the constituent quarks or the current quarks (see related discussion in [55]). In order to resolve quark degrees of freedom inside a hadron, the transverse momentum  $p_T$  in a process should be higher than  $p_T^0$ . That could be the reason for the  $p_T$  dependence of polarization (19).

## 10 Discussion

The results of the previous sections indicate that the use of two scaling variables  $x_{A\pm} = (x_R \pm x_F)/2$  is essential for the universal energy independent description of the existing hyperon polarization data in inclusive reactions. The scaling variables transform into each other under rotation transformation around the normal to the scattering plane and allow one to satisfy in a natural way the feature (5), which is also related with the rotation invariance. The variables  $x_{A\pm}$  treat on a more equal basis the data for the central and the fragmentation regions as well as the transverse and the longitudinal

momentum components of the produced hyperon.

The form of eq. (10) is chosen from the dimensional analysis, the rotation invariance requirement and it is also motivated by the existing data for both the hyperon polarization and the analyzing power in inclusive reactions for hadron-hadron collisions. The derived formulas are applicable for both the  $A_N$  and the  $\mathbf{P}_H$  data approximation and reflect the scaling properties of these two classes of processes at high enough energies and  $p_T$ . The specific range of energies and  $p_T$  at which the scaling properties are valid could depend on the process type. The existence of the above scaling implies that large spin effects will survive at high energies and do not depend directly on the beam energy. These properties of the  $A_N$  and the  $\mathbf{P}_H$  are waiting for their explanation in the strong interaction theory in general and in the Quantum Chromodynamics (QCD) in particular.

## 10.1 Analogy between the scaling properties of hyperon polarization and the analyzing power

It is important to take into account in the future models a deep analogy between the hyperon polarization and the analyzing power, which follows from the results of this study and [47, 48, 49]. Below we list some common features of the  $A_N$  and the  $\mathbf{P}_H$ , which indicate a common nature of both phenomena.

Features of the analyzing power in inclusive hadron production by polarized protons and antiprotons and features of the hyperon polarization in inclusive hadron-nucleon collisions:

- a) Scaling behaviour for the hyperon polarization and the analyzing power as a function of  $x_{A\pm} = (x_R \pm x_F)/2$  and  $p_T$  in the beam fragmentation region, and in the central region.
- b) The  $\mathbf{P}_H$  and the  $A_N$  are approximated by a product of functions of  $p_T$  and  $x_{A\pm}$ :  $\mathbf{P}_H = F(p_T)[G(x_{A+} - x_2) - \sigma G(x_{A-} + x_2)]$ , where the  $x_2$  could depend on  $p_T$  and a reaction type.
- c) The function  $F(p_T)$  rises with  $p_T$  at small  $p_T \leq p_T^0$  and have a plateau or decrease above  $p_T^0$ , where  $p_T^0 = 0.4-2$  GeV/c depends on a reaction type.

- d) The function  $G(x_{A\pm})$  is proportional to  $\sin[\omega(x_{A\pm} - x_1)]$ , where  $x_1$  could depend on  $p_T$ . The  $\omega$  is a universal function of quantum numbers characterizing the reaction, common for the  $\mathbf{P_H}$  and  $A_N$ .
- e) The  $\mathbf{P_H}$  and the  $A_N$  are zero at  $p_T = 0$  due to the absence of a preferable direction, such as a normal to the scattering plane. This implies  $F(0) = 0$ .
- f) The sign and the magnitude of the  $\mathbf{P_H}$  and the  $A_N$  depend on the projectile, the target, and the produced hadron flavors.

We may conclude that a close similarity of the kinematic behaviour of  $\mathbf{P_H}$  and  $A_N$  and a universal dependence of the  $\omega$  parameter on quantum numbers indicate on a common origin of spin effects in these two classes of spin-dependent reactions.

## 10.2 Interference origin of the hyperon polarization

The polarization of hadrons is a pure Quantum mechanics effect related with the interference of spin-flip ( $g$ ) and spin-nonflip ( $f$ ) amplitudes. The transverse hadron polarization can be expressed via the  $f$  and  $g$  amplitudes as [56]

$$\mathbf{P_H} = 2Im(f^*g)/(|f|^2 + |g|^2). \quad (40)$$

Taking into account eqs. (10)- (12) we can choose amplitudes  $f$  and  $g$  as

$$f \propto f_0 \{ \exp[-i\omega(x_{A+} - x_1 - x_2)/2] + (\sqrt{\sigma})^* \exp[-i\omega(x_{A-} - x_1 + x_2)/2] \}, \quad (41)$$

$$g \propto g_0 \frac{c}{2\omega} A^\alpha F(p_T) \{ \exp[i\omega(x_{A+} - x_1 - x_2)/2] - \sqrt{\sigma} \exp[i\omega(x_{A-} - x_1 + x_2)/2] \}, \quad (42)$$

where  $f_0$  and  $g_0$  are the functions of kinematic variables ( $x_F$ ,  $p_T$ ,  $\sqrt{s}$ ) with zero relative phases, which have to satisfy the constraints followed from both the polarization and the cross section data. The generalized optical theorem predicts the following relation for a cross section:

$$\mathbf{P_H} d\sigma = 2Im(f^*g), \quad (43)$$

where  $d\sigma$  is the corresponding unpolarized inclusive cross section [46], which can be used together with eq. (40) to fix the  $f_0$  and  $g_0$ .



To have a non-zero value of the  $\mathbf{P}_H$  both amplitudes have to be non-zero and the phase difference  $\Delta\phi$  between spin-flip and spin-nonflip amplitudes has to be non-zero too. For the cases of  $\sigma = \pm 1$  the following phase differences are expected from eqs. (41)-(42):

$$\Delta\phi = (1 + \sigma)\pi/4 + \omega(x_R w_1 - x_1) + \text{Arg}(c/\omega). \quad (44)$$

As we can see from eq. (44), the variables  $x_R$  and  $\omega$  play an important role in the hyperon polarization phenomena since they determinate the phase difference between the spin-flip and non-flip amplitudes. The higher is the  $\omega$  value, the larger the  $\Delta\phi$  change rate with the  $x_R$  increase. Eq. (21) for  $\omega_Q$  can be considered as a sum of effective “charges”, which create a mean field and lead to the change of the phase difference  $\Delta\phi$ .

In the lowest-order perturbative  $QCD$  all amplitudes are relatively real. This tends to rule out polarization in the hard scattering of partons, which seems to be well described in the low-order  $QCD$ . The observation of undiminished polarization near  $p_T = 4$  GeV/c implies that either perturbative  $QCD$  does not apply or that another mechanism is responsible, such as interference of excited states or the fragmentation process [11].

### 10.3 Some theoretical ideas for hyperon polarization

Several phenomenological models have been proposed to explain the hyperon polarization data and the analyzing power data (see recent review in [46]). Some of the models have the features that allow one to understand, at least at a qualitative level, the analogy between the  $A_N$  and the  $\mathbf{P}_H$  discussed above.

#### 10.3.1 Orbital motion of valence quarks

One class of such models assumes that an orbital motion of valence quarks and surface effects are responsible for the correlation between the quark spin direction and transverse motion of produced hadron [49, 55]. By taking the  $\Lambda$ 's containing two, one or zero valence quark(s) of a beam proton into account, the model predicts the sign and the  $x_F$  dependence of  $\Lambda$ 's polarization. The model predicts correctly the sign and the magnitude of  $\Sigma^-$ ,  $\Xi^{0,-}$  polarization in  $pp$  collisions, and  $\Lambda$  polarization in  $K^-p$  collisions. It also predicts a smaller magnitude for  $\Lambda$ 's produced by  $\pi^\pm$  beams. The authors of

the model claim an analogy of mechanisms, which lead to non-zero hyperon polarization and analyzing power. The model does not explain the specific features of antihyperon polarization.

### 10.3.2 Parton rotation inside constituent quarks

A separate approach was developed by Troshin and Tyurin, which assumes the rotation of a quark-antiquark cloud inside constituent quarks [57, 58]. The main role belongs to the orbital angular momentum and polarization of the strange quark-antiquark pairs in the internal structure of constituent quarks. The hyperons are produced in two stages. At the first stage the overlapping and interaction of peripheral clouds occur which results in massive quark appearance and a mean field is generated. Constituent quarks located in the central part of hadron are supposed to scatter in a quasi-independent way by this mean field. At the second stage two mechanisms take place: Recombination of the constituent quarks with a virtual massive strange quark (soft interaction) into a hyperon or a scattering of a constituent quark in the mean field, excitation of this constituent quark, appearance of a strange quark as a result of decay of the constituent quark and a subsequent fragmentation of a strange quark into a hyperon (high  $p_T$ 's hard interaction). The resulting expression at  $p_T > 1$  GeV/c when hard interactions dominate is

$$P(s, x, p_T) \simeq \sin[P_q < L_{\bar{q}q} >], \quad (45)$$

where  $P_q$  is the polarization of the constituent quark  $q$  which arises due to multiple scattering in the mean field and  $< L_{\bar{q}q} >$  is the mean value of an internal angular momentum inside the constituent quark.

Thus, in this model the polarization of a strange quark is the result of multiple scattering of a parent constituent quark, the correlation between the polarization of a strange quark and the polarization of the constituent quark and a local compensation of a spin and an orbital angular momentum of a strange quark.

The simplest possible  $x$  dependence of  $P_q$  is taken

$$P_q(x) = P_q^{max} x, \quad (46)$$

where  $P_q^{max} = -1$ .

The model predicts the negative sign and  $x_F$  dependence of the  $\Lambda$  polarization. Eq. (45) resembles eq. (12), especially in the beam fragmentation

region, with effective  $\omega = \langle L_{\bar{q}q} \rangle$ . Eqs. (45), (46) predicts a scaling behaviour of the hyperon polarization. The concept of the mean field, generated by quarks, which leads to a hyperon polarization and to its change with  $x$  rise similar to eq. 12 is also in consent with the analysis, presented above.

There are no predictions for other hyperons, though the authors assume zero polarization in inclusive process  $pp \rightarrow p + X$  due to a low probability of multiple scattering in the mean field in comparison with a single scattering. A single scattering does not polarize quarks and protons appear unpolarized in the final state since a single scattering is dominant in this process.

There are several semiclassical models, which provide simple arguments for a qualitative description of the hyperon polarization, but since they fully ignore the relevance of the phase difference, which is crucial, they are unable to make solid quantitative predictions.

### 10.3.3 The recombination model

In the recombination model [59, 60] a dynamical reason for the spin-momentum correlation is explained by the effect of Thomas precession [61, 62]. The effect arises when the direction of the force acting on a quark does not coincide with the direction of its motion. It leads to a rotation of the quark spin and could be the reason of the discussed above “oscillation” of polarization or analyzing power as a function of  $x_F$ . The Thomas frequency is an inverse function of a quark mass

$$\vec{\omega}_T = \frac{\gamma}{\gamma + 1} \frac{\vec{F}}{m_q} \times \vec{V}, \quad (47)$$

where  $V$  is the strange quark velocity,  $F$  - the force,  $m_q$  - the strange quark mass, and  $\gamma = (1 - V^2)^{-1/2}$ . An additional term will appear in the effective Hamiltonian which describes the recombination process

$$U = \vec{S} \cdot \vec{\omega}_T, \quad (48)$$

where  $\vec{S}$  is a spin of the quark. Within the old-fashioned perturbation theory the final expression for the  $\Lambda$  polarization is

$$P(p \rightarrow \Lambda) = -\frac{12p_T x_F (x_F - 3x_s)}{\Delta x_0 M^2 (x_F + 3x_s)^2}, \quad (49)$$

where it is assumed that a recombination time  $\Delta t \approx (p_z^{ave}/m_q)\Delta x_0$ , the average momentum of the quark is  $p_z^{ave} \approx P(x_F + 3x_s)/6$  and  $\Delta x_0 \approx 4 \text{ GeV}^{-1}$  is a distance scale of the order of the proton radius. The  $M \simeq 2 \text{ GeV}/c^2$  is an effective mass and the  $x_s$  is a fraction of a proton momentum ( $P$ ) which carries the  $s$  quark [59]. These assumptions lead to a quark mass cancellation in the polarization formula (49) and a scaling behaviour of the  $\Lambda$  polarization. The model gives the right sign and a good approximation of the  $x_F$  dependence for the  $\Lambda$  polarization. There are also many predictions for hyperon polarization in other reactions. They are based on some rules which are formulated within the framework of the recombination model. In particular, there is a statement that the effect of recombination of the partons in the proton as they are transferred into the outgoing hadron may be different depending on whether they are accelerated (as are the slow sea partons) or decelerated (as are the fast valence partons). It is also a statement that two partons with similar wave functions in the proton may interact with themselves differently not as they interact with a parton whose wave function is different. This results in a simple rule: slow partons preferentially recombine with their spins down in the scattering plane while fast partons recombine with their spins up.

The model predicts correctly the polarization sign but not the magnitude for some of the reaction. So, the model predicts the same polarization magnitude for  $p \rightarrow \Lambda$  as it is for  $p \rightarrow \Xi^{-,0}$ , but we know from the above analysis that the polarization magnitudes for  $\Xi^{-,0}$  are two times smaller. Similarly, for  $K^- p \rightarrow \Lambda$  process the model predicts the same magnitude as for  $p \rightarrow \Lambda$ , while the measured value is two times larger. Since the polarization in the model is essentially kinematic at the quark level all the antibaryons should have zero polarization. As we have seen in the above analysis, the experimental situation is much more complicated.

There is another estimate of the hadronization time which follows from the analysis of  $A$ -dependence of hadron production  $\Delta t \approx p^c/M_0^2$ , where  $M_0 \approx 1 \text{ GeV}$  [63]. The use of this  $\Delta t$  estimate results in a different expression for the  $\Lambda$  polarization

$$P(p \rightarrow \Lambda) = -\frac{2p_T M_0^2 x_F (x_F - 3x_s)}{m_q M^2 x_R (x_F + 3x_s)}, \quad (50)$$

which is an inverse function of the  $s$  quark mass  $m_q$ . This example shows that the hyperon polarization is sensitive to the details of the hadronization

process. These results seem to imply that the origin of hyperon polarization is closely related with the confinement mechanism.

Since the Thomas precession frequency is an inverse function of the quark mass  $m_q$ , this may be the reason for a large variation of the  $\omega_Q$  parameter for different reactions. The ratio  $m_s/m_d$  is estimated to be from 17 to 25 with a mean about 21 [64]. The same order of magnitude is given by the ratio  $65.19/3.045 = 21.4$  of the  $\omega_Q$  parameters for the processes  $p \rightarrow \Xi^+$  and  $p \rightarrow \Lambda$ , in which  $s$  and  $\bar{d}$  quarks play an important role. It is interesting to estimate the total rotation angle of a quark spin using the above approximations

$$\phi_{rot} = \omega_T \Delta t \approx \frac{p_T \cdot (x_F - 3x_s)}{m_q \cdot (x_F + 3x_s)}. \quad (51)$$

Taking typical  $x_F = 0.7$ ,  $x_s = 0.1$ ,  $p_T = 1$  GeV/c, and  $m_s = 122$  MeV/c<sup>2</sup>, we have  $\phi_{rot} = 3.3$ , while for the  $d$  quark with  $m_d = 6$  MeV/c<sup>2</sup> the  $\phi_{rot} = 67$ . So, the total rotation angle of a quark spin due to the Thomas precession could be rather large and varies in the same range as that of the  $\omega_Q$ .

In case of  $\Xi^-$  and  $\Xi^0$  production in  $pp$  collisions the effective field created by the spectator quarks  $\propto n_q(a\bar{c})$  is expected to be two times higher than for  $\Lambda$  production and the corresponding rotation angle will be also two times larger, in agreement with the  $\omega$  value for  $\Xi^-$  and  $\Xi^0$  production.

### 10.3.4 Lund model

Another explanation of spin-momentum correlation follows from a picture of a colour flux tube, which emerges after the collision between an outgoing quark and the rest of hadronic system [65, 66]. The  $SU(6)$  wave function is assumed for hadrons, in particular, for  $\Lambda$  the  $(ud)$  system is in a singlet state, so the  $\Lambda$  polarization is that of the  $s$  quark. An outgoing  $ud$  diquark with spin  $S = 0$  and isospin  $I = 0$  stretches the colour field and a  $s\bar{s}$  pair is produced. It is assumed that the  $s$  quark has  $p_T$  which must be locally compensated by that of the  $\bar{s}$  quark. As a result, the  $s\bar{s}$  pair has an orbital momentum which is assumed to be balanced by the spin of the  $s\bar{s}$  pair. The model predicts a negative  $\Lambda$  polarization in  $pp$  collisions but cannot predict its magnitude or  $x_F$  dependence. The  $p_T$  dependence of the polarization is linear. The model needs additional assumptions to explain the polarization in other reactions and fails to explain the antihyperon polarization.

### 10.3.5 Optical approximation

We propose a simple toy model which uses an analogy with the optics. Let us consider the  $\Xi^-$  production in a collision of two protons ( $a$  and  $b$ ) in their c.m. reference frame. The proton's longitudinal size is about  $2R_h/\gamma_{cm}$ , where  $R_h \approx 0.8$  fm is a proton radius and  $\gamma_{cm} = E_{cm}/(2m_p c^2)$ .

In an optical picture the phase can be related with the number of scattering centers [67]. We assume here that a hadron can be characterized by an effective refractive index ( $n$ ) which leads to a phase difference  $\chi = (n-1)d \cdot p_q/\hbar$  between spin-flip and spin-nonflip quark scattering amplitudes, where  $d$  is a total path length inside a proton and  $p_q \approx p_c/z \approx p_a x_R/z$  is a quark momentum. It is assumed here for the sake of simplicity that a quark from the proton  $a$  passes on average half of the proton  $b$  thickness and then changes its angle due to a scattering in the proton  $b$ . The second part of its way inside the proton is approximately by a factor of  $1/\cos\theta_{cm} = x_R/x_F$  larger than that before the scattering (we consider here not too large scattering angles). This results in a phase difference

$$\chi_a \approx \frac{R_h(n-1)x_R}{\lambda_p < z > x_F} (x_F + x_R), \quad (52)$$

where  $\lambda_p = \hbar/(m_p c) \approx 0.210$  fm is the proton Compton wavelength. Eq. (52) can be rewritten as  $\chi_a = \omega_{eff} \cdot x_{A+}$ , where

$$\omega_{eff} = \frac{2R_h(n-1)x_R}{\lambda_p < z > x_F}, \quad (53)$$

and  $< z >$  is the mean fraction of a quark momentum which is carried by the produced hyperon. A similar consideration of the proton  $b$  quark scattering inside the proton  $a$  results in a  $\chi_b = \omega_{eff} \cdot x_{A-}$  and the total contribution into the  $\Xi^-$  polarization is

$$\mathbf{P}_{\Xi-} \propto [\sin(\omega_{eff} \cdot x_{A+}) - \sin(\omega_{eff} \cdot x_{A-})], \quad (54)$$

which is very similar to eq. (10). The averaging over the transverse quark coordinates inside a proton is not taken into account for the sake of simplicity. A more careful consideration of a quark path length after the scattering removes the singularity  $1/x_F$  in eq. (54) since the path length is limited at  $\theta_{cm} = \pi/2$  by the  $R_h$ . The  $p_T$  dependence of a hyperon polarization is

also not taken into account in eq. (54) since we assume that  $p_T$  is high enough to resolve quarks inside the hadron structure. The condition for that is  $p_T \geq \hbar/r_q \approx 3\hbar/R_h \approx 0.75$  GeV/c, where  $r_q$  is a constituent quark radius. Comparison of eqs. (53) and (21) assumes that  $(n-1) \propto \omega_Q \propto n_q(a\bar{c})$ .

We may learn from this toy model that the hyperon polarization oscillation is probably related with a corresponding scattering amplitude phase change due to the hadron mean field generated during hadron interaction. The field strength is proportional to the number of scattering centers  $n_q(a\bar{c})$  in agreement with the above analysis of experimental data. The scaling variables  $x_{A+}$  and  $x_{A-}$  arise in this model from the consideration of geometrical and relativistic properties of interacting hadrons and the assumption that the phase difference  $\chi$  is proportional to the quark path length in the mean hadron field.

## 11 Conclusion

The analysis of experimental data on the hyperon and antihyperon polarization has been made. It is shown that the existing (anti)hyperon polarization data in inclusive reactions for  $pp(A)$ ,  $\pi^\pm p$ ,  $K^\pm p$ ,  $\bar{p}p$  and hyperon-nucleon collisions can be described by a function of  $p_T$  and two scaling variables  $x_{A\pm} = (x_R \pm x_F)/2$ :  $\mathbf{P}_H = A^\alpha F(p_T)[G(x_{A+} - x_2) - \sigma G(x_{A-} + x_2)]$ . The function  $G(x_{A\pm})$  is approximated in the scaling limit by a simple expression  $\propto \sin[\omega(x_{A\pm} - x_1)]$  which results in an oscillation of polarization in case of large  $\omega$  value. Functions  $F(p_T)$ ,  $x_1$ , and  $x_2$  depend on  $p_T$  and can be approximated by constants above 1-2 GeV/c.

It is found that the  $\omega$  parameter is consistent with an universal dependence on quark composition (eq. (21)) for about two tens measured (anti)baryon production processes. In addition, the preliminary analysis indicates the validity of the same eq. (21) for about two dozen spin-dependent processes in which analyzing power of produced hadrons was measured. Universal character of the  $\omega$  dependence on quantum numbers allows one to predict the  $\omega$  values for a large number of processes in which analyzing power or hadron polarization is measured. It indicates also that we deal with a physical case and not just with data description.

In particular, we expect a near linear dependence of the analyzing power on  $x_F$  for  $\pi, K$  production in  $p^\uparrow p$  and  $\bar{p}^\uparrow p$  collisions due to a small value of

$\omega \approx 0.98$ .

The polarization of  $\bar{\Lambda}$  in  $\bar{p}p$  collisions is fitted well by eq. (10) and indicates an oscillation of it as a function of  $x_F$ . Similar oscillations with large  $\omega$  parameter are also seen for other processes, including  $\Xi^0 \rightarrow \Xi^-$  and  $p \rightarrow \Omega^-$ .

The data fits indicate a simple relation for the  $\omega$  parameter in case of hyperons produced in  $pp$  collisions:  $\omega \approx 1.5n_q(a\bar{c})$ , where  $n_q(a\bar{c})$  is the number of quarks in the  $a\bar{c}$  system.

The data fits indicate also that the  $\Lambda$  hyperon polarization decreases on nuclear targets according to the law  $\mathbf{P}_H \propto A^{\alpha_1|x_F|}$ , with  $\alpha_1 \approx -0.16$ . This effect may be related with the rescattering of polarized  $s$  quarks in the nuclear matter before formation of a hyperon is over. Since the formation length is proportional to the final hyperon momentum, we expect a rise of  $s$  quark rescattering probability with  $|x_F|$  increase. Due to the similarity between the hyperon polarization and the analyzing power features we expect that the  $A$ -dependence of the analyzing power is also described by the law  $A_N \propto A^{\alpha_1|x_F|}$  with  $\alpha_1 \approx -(0.1 \div 0.3)$ .

The polarization sign and its magnitude depend on quark composition of hadrons participating in the reaction and can be predicted using the proposed formulas. In most cases the processes with large  $\omega$  value have a small magnitude which makes it difficult to measure.

There is an analogy between the scaling properties of polarization for hyperons, produced in collisions of unpolarized hadrons, and the scaling properties of the analyzing power of hadrons, produced in the collisions of polarized protons (antiprotons) with hadrons. This analogy between the analyzing power and the hyperon polarization indicates on a common origin of both phenomena. The possible mechanism may be related with the confinement forces. These forces are created by the mean colour field generated after the initial hard scattering of quarks. The quark spin rotation in the mean field could lead to the phase difference between spin-flip and spin-nonflip amplitudes which results in the hyperon polarization.

The origin of the scaling variables  $x_{A\pm} = (x_F \pm x_R)/2$  can be understood from the dimensional analysis, the rotational invariance, and also in the framework of an optical picture of hadron-hadron interactions.



## References

- [1] G. Bunce et al., *Phys. Rev. Lett.* **36** (1976) 1113.
- [2] F. Abe et al., *Phys. Rev.* **D34** (1986) 1950.
- [3] F. Abe et al., *Phys. Rev. Lett.* **50** (1983) 1102.
- [4] B.E. Bonner et al., *Phys. Rev.* **D38** (1988) 729.
- [5] E.C. Dukes et al., *Phys.Lett.* **B193** (1987) 135.
- [6] K. Raychaudhuri et al., *Phys. Lett.* **90 B** (1980) 319.
- [7] S.A. Gourlay et al., *Phys. Rev. Lett.* **56** (1986) 2244.
- [8] C. Wilkinson et al., *Phys. Rev. Lett.* **46** (1981) 803.
- [9] K. Heller et al., *Phys. Rev. Lett.* **51** (1983) 2025.
- [10] K. Heller et al., *Phys. Rev. Lett.* **41** (1978) 607.
- [11] B. Lundberg et al., *Phys. Rev.* **D 40** (1989) 3557.
- [12] E.J. Ramberg et al., *Phys. Lett.* **338 B** (1994) 403.
- [13] A.M. Smith et al., *Phys. Lett.* **185** (1987) 209.
- [14] A. Morelos et al., *Phys. Rev. Lett.* **71** (1993) 2172.
- [15] C. Wilkinson et al., *Phys. Rev. Lett.* **58** (1987) 855.
- [16] C. Ankenbrandt et al., *Phys. Rev. Lett.* **51** (1983) 863.
- [17] Y.W. Wah et al., *Phys. Rev. Lett.* **55** (1985) 2551.
- [18] L. Deck et al., *Phys. Rev.* **D 28** (1983) 1.
- [19] B.E. Bonner et al., *Phys. Rev. Lett.* **62** (1989) 1591.
- [20] J. Duryea et al., *Phys. Rev. Lett.* **67** (1991) 1193.
- [21] P.M. Ho et al., *Phys. Rev. Lett.* **65** (1990) 1713.

- [22] L.H. Trost et al., *Phys. Rev. D* **40** (1989) 1703.
- [23] R. Rameika et al., *Phys. Rev. D* **33** (1986) 3172.
- [24] M.L.Faccini-Turleur et al., *Z. Phys. C* **1** (1979) 19.
- [25] A.Borg et al., *Nuovo Cimento* **22 A** (1974) 559.
- [26] H. Abramowicz et al., *Nucl. Phys. B* **105** (1976) 222.
- [27] H. Grassler et al., *Nucl. Phys. B* **136** (1978) 386.
- [28] M. Baubillier et al., *Nucl. Phys. B* **148** (1979) 18.
- [29] J. Bensinger et al., *Nucl. Phys. B* **252** (1985) 561.
- [30] S.N. Ganguli et al., *Nucl. Phys. B* **128** (1977) 408.
- [31] P.V. Chliapnikov et al., *Nucl. Phys. B* **112** (1976) 1.
- [32] W. Barletta et al., *Nucl. Phys. B* **51** (1973) 499.
- [33] I.V. Ajinenko et al., *Phys. Lett.* **121 B** (1983) 183.
- [34] B. Adeva et al., *Z. Phys. C* **26** (1984) 359.
- [35] R. Sugahara et al., *Nucl. Phys. B* **156** (1979) 237.
- [36] F. Barreiro et al., *Phys. Rev. D* **17** (1978) 669.
- [37] J. Bensinger et al., *Phys. Rev. Lett.* **50** (1983) 313.
- [38] P.H. Stuntebeck et al., *Phys. Rev. D* **9** (1974) 608.
- [39] K. Heller, In Proceeding of the 12th International Symposium on High-Energy Spin Physics, September 10 - 14, 1996. Amsterdam, The Netherlands. Ed. by C.W. de Jager et al. World Sci., Singapore. (p. 23) 1996.
- [40] K.B. Luk et al., *Phys. Rev. Lett.* **70** (1993) 900.
- [41] M.I. Adamovich et al., *Z. Phys. A* **350** (1995) 379.
- [42] R.O. Polvado et al., *Phys. Rev. Lett.* **42** (1979) 1325.

- [43] G.L. Kane, J. Pumplin and W. Repko, *Phys. Rev. Lett.* **41** (1978) 1689.
- [44] L.G. Pondrom, *Phys. Rep.* **122** (1985) 57.
- [45] J.Lach, Hyperon Polarization and Magnetic Moments. Preprint FERMILAB-Conf-93/381. 1993.
- [46] J.Soffer, Is the riddle of the hyperon polarization solved?, (Marseille, CPT). Preprint CPT-99-P-3898, Sep. 1999. Invited talk at Hyperon 99: Hyperon Physics Symposium, Batavia, Illinois, 27-29 Sep. 1999. p. 121; hep-ph/9911373 (1999).
- [47] V.V. Abramov, A New Scaling for Single-Spin Asymmetry in Meson and Baryon Hadroproduction. IHEP Preprint 98-84, Protvino, 1998; hep-ph/0110152.
- [48] V.V. Abramov, *Eur. Phys. J. C* **14** (2000) 427; DOI 10.1007/s100529900355.
- [49] Liang Zuo-tang and C.Boros, *Phys. Rev. Lett.* **79** (1997) 3608.
- [50] Yu. Bushnin et al., *Phys. Lett.* **29** (1969) 48.
- [51] J. Felix et al., *Phys. Rev. Lett.* **76** (1996) 22.
- [52] R. Blankenbeckler and S.J. Brodsky, *Phys. Rev. D* **10** (1974) 2973.
- [53] J. Qui and G. Sterman, Preprint ITP-SB-98-28; *Phys. Rev. D* **59** (1999) 014004; hep-ph/9806356. Single Transverse Spin Asymmetries in Hadronic Pion Production.
- [54] J. Franklin, *Phys. Rev.* **172** (1968) 1807.
- [55] C. Boros, Liang Zuo-tang, *Phys. Rev. D* **57** (1998) 4491.
- [56] M.G. Ryskin, Polarization phenomena and confinement forces, In Proc. of the Int. Conf. on Quark Confinement and the Hadron Spectrum, Como, Italy, 20-24 June 1994. Edited by N.Brambilla and G.M.Proserpi. River Edge, N.J., World Scientific, 1995, p. 261.
- [57] S.M. Troshin and N.E. Tyurin, *Phys. Rev. D* **55** (1997) 1265.

- [58] S.M. Troshin and N.E. Tyurin, *Phys. Rev. D* **52** (1995) 3862.
- [59] T.A. DeGrand, H. Miettinen, *Phys. Rev. D* **24** (1981) 2419.
- [60] T.A. DeGrand et al., *Phys. Rev. D* **32** (1985) 2445.
- [61] L.T. Thomas, *Philos. Mag.* **3** (1927) 1.
- [62] A.A. Logunov, *On Tomas Precession*. IHEP preprint 98-85, Protvino, 1998.
- [63] V.V. Abramov, *Yad. Fiz.* **44** (1986) 1318 [*Sov. J. Nucl. Phys.* **44** (1986) 856].
- [64] D.E.Groom et al., *Eur. Phys. J. C* **15** (2000) 1.
- [65] B. Anderson, G. Gustafson and G. Ingelman, *Phys. Lett. B* **85** (1979) 417; *Phys. Rep.* **97** (1983) 31.
- [66] M.G. Ryskin, *Yad. Fiz.* **48** (1988) 1114 [*Sov. J. Nucl. Phys.* **48** (1988) 708].
- [67] S.M. Troshin, N.E. Tyurin, *Uspechi Fiz. Nauk* **164** (1994) 1073.

Table 10: The comparison of the estimated  $\omega$  parameter and its prediction  $\omega_Q$  from eq. (22). The estimate of maximum in hyperon polarization magnitude using the fit parameters of eq. (10)-(20). The maximum is estimated for the  $x_F \geq 0$  region.

#	reaction	$Q_1$	$Q_2$	$Q_3$	$Q_4$	$\omega$	$\omega_Q$	$\mathbf{P}_H^{\max}$	$P_Q$
1	$pBe \rightarrow \Lambda$	2	0	0	0	$3.13 \pm 0.24$	3.045	$-0.272 \pm 0.011$	-0.275
2	$pBe \rightarrow \Xi^0$	4	0	0	0	$6.10 \pm 0.92$	6.090	$-0.141 \pm 0.052$	-0.138
3	$pBe \rightarrow \Xi^-$	4	0	0	0	$5.95 \pm 0.74$	6.090	$-0.140 \pm 0.021$	-0.138
4	$pBe \rightarrow \Sigma^+$	2	0	0	0	$1.9 \pm 1.2$	3.045	$0.337 \pm 0.076$	0.275
5	$pBe \rightarrow \Sigma^-$	4	0	0	0	$6.1 \pm 4.0$	6.090	$0.34 \pm 0.26$	0.275
6	$K^-p \rightarrow \Lambda$	3	-1	0	0	$3.53 \pm 0.22$	3.58	$0.61 \pm 0.11$	0.604
7	$K^-p \rightarrow \Xi^-$	3	-1	0	0	$3.04 \pm 0.88$	3.58	$0.53 \pm 0.17$	0.604
8	$K^+p \rightarrow \Lambda$	3	-1	0	0	$4.4 \pm 1.5$	3.58	$\pm 0.23 \pm 0.15$	-0.052
9	$\pi^-p \rightarrow \Lambda$	3	-1	0	0	$4.33 \pm 0.94$	3.58	$\pm 0.23 \pm 0.14$	-0.178
10	$\pi^+p \rightarrow \Lambda$	3	-1	0	0	$5.2 \pm 6.5$	3.58	$\pm 0.14 \pm 0.17$	-0.178
11	$K^-p \rightarrow \bar{\Lambda}$	3	1	0	0		5.55	$0.4 \pm 0.4$	0.302
12	$K^+p \rightarrow \bar{\Lambda}$	3	1	0	0	$4.4 \pm 1.9$	5.55	$0.78 \pm 0.25$	0.604
13	$pBe \rightarrow \bar{\Lambda}$	6	2	2	0	$18.5 \pm 5.7$	22.27	$\pm 0.021 \pm 0.010$	-0.025
14	$\bar{p}Be \rightarrow \bar{\Lambda}$	2	0	2	0	$16.2 \pm 4.1$	14.21	$\pm 0.187 \pm 0.046$	0.194
15	$pBe \rightarrow \Xi^+$	6	2	2	1		65.19	$\pm 0.18 \pm 0.03$	-0.188
16	$\Xi^0 Be \rightarrow \Xi^-$	2	0	0	1	$46.0 \pm 3.7$	45.97	$\pm 0.026 \pm 0.005$	0.022
17	$\Sigma^- C \rightarrow \Xi^-$	2	0	0	0	$3.3 \pm 3.5$	3.045	$-0.4 \pm 0.4$	-0.275
18	$\Lambda Be \rightarrow \Omega^-$	4	0	0	0		6.090	$0.111 \pm 0.067$	0.132
19	$pp(C) \rightarrow p$	4	0	0	0	$6.12 \pm 0.21$	6.090	$\pm 0.072 \pm 0.014$	0.072
20	$pBe \rightarrow \Omega^-$	6	2	2	0		22.27	$0.032 \pm 0.016$	0.031
21	$pCu \rightarrow \bar{\Sigma}^-$	6	2	2	0		22.27	$0.088 \pm 0.011$	0.092
22	$pBe \rightarrow \Sigma^0$	2	0	0	0		3.045	$0.28 \pm 0.13$	0.275

Table 11: The fit parameters of eqs. (21) and (32).

$a_1$	$a_2$	$a_3$	$a_4$	$a_5$	$\chi^2/N_{DOF}$
$1.523 \pm 0.045$	$0.98 \pm 0.24$	$5.6 \pm 1.70$	$43.0 \pm 3.7$	$\approx 12$	$3.57/12$
$b_1$	$b_2$	$b_3$	$b_4$	$b_5$	$\chi^2/N_{DOF}$
$0.70 \pm 0.19$	$0.545 \pm 0.066$	$4.94 \pm 0.73$	$11.6 \pm 1.5$	$-4.73 \pm 0.74$	$5.5/16$

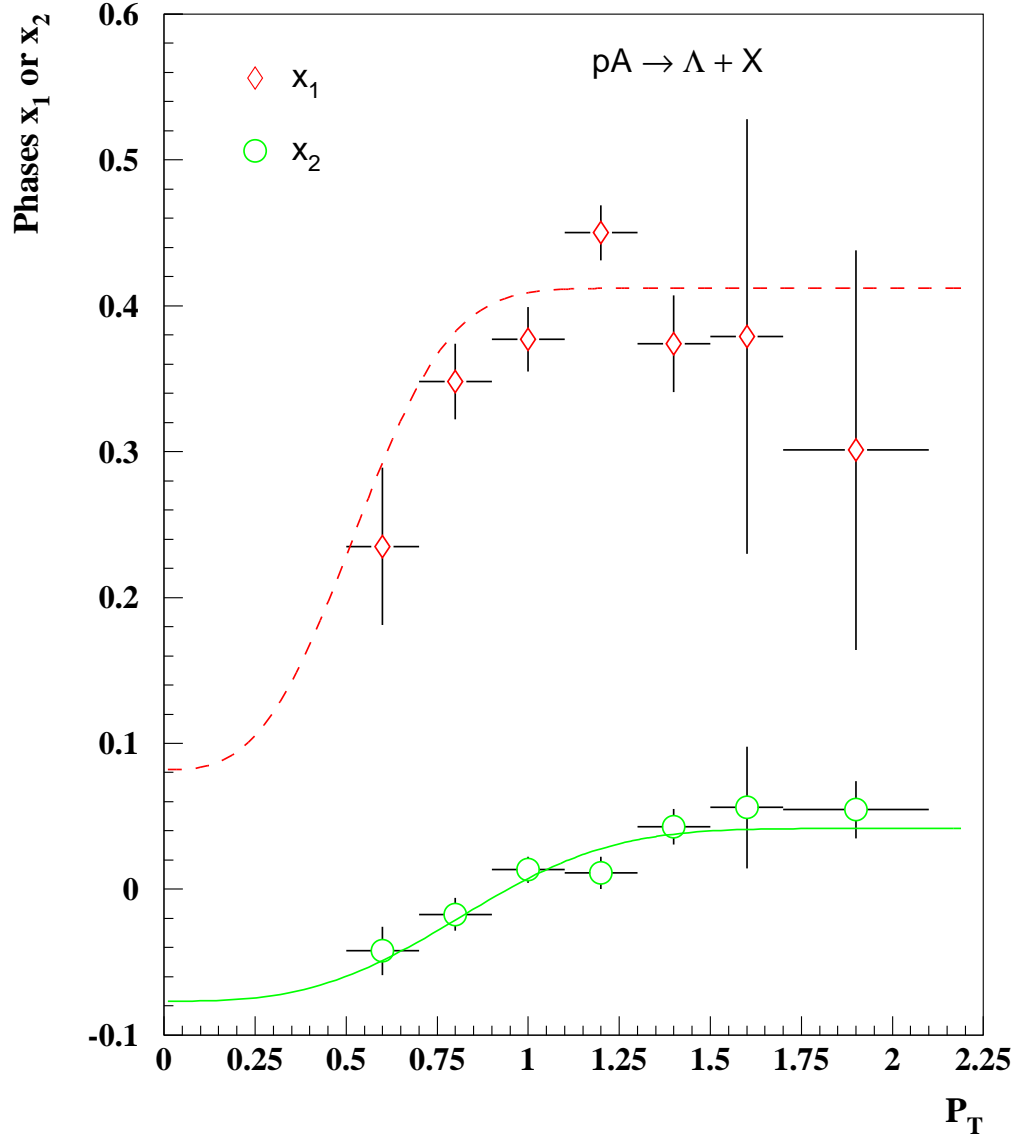


Figure 1: The dependence of  $x_1$  and  $x_2$  parameters on  $p_T$  for  $\Lambda$  production in  $pp(A)$  collisions. The curves correspond to eq. (13) (dashed) and eq. (14) (dash-dotted), respectively.

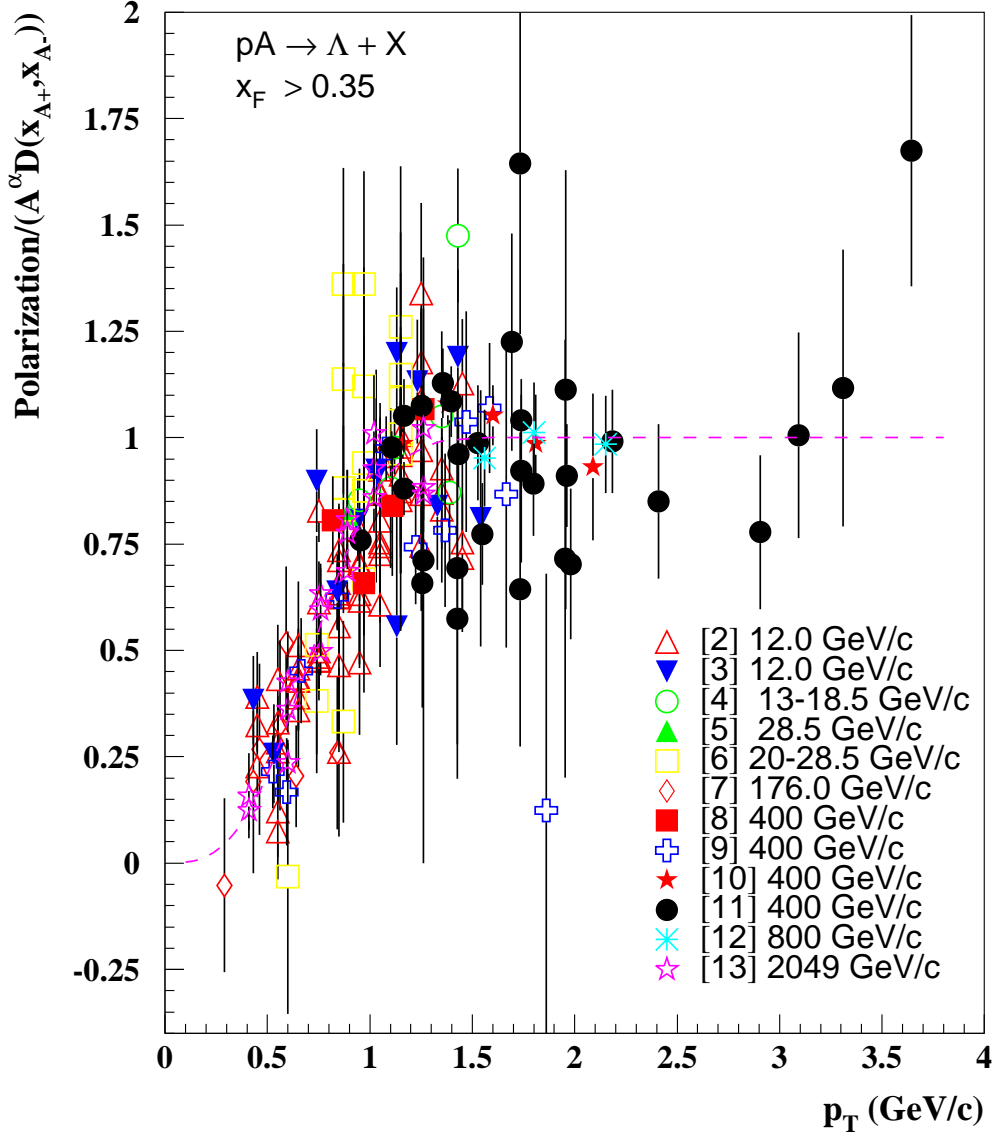


Figure 2: The ratio of polarization and  $A^\alpha D(x_{A+}, x_{A-})$ , (eq. (18)) vs  $p_T$  for  $\Lambda$  production in  $pp(A)$  collisions, and  $x_F \geq 0.35$ . Parameters of eqs. (10)-(15) are presented in Table 1, fit # 2. The curve corresponds to the function  $F(p_T)$  in eq. (10).



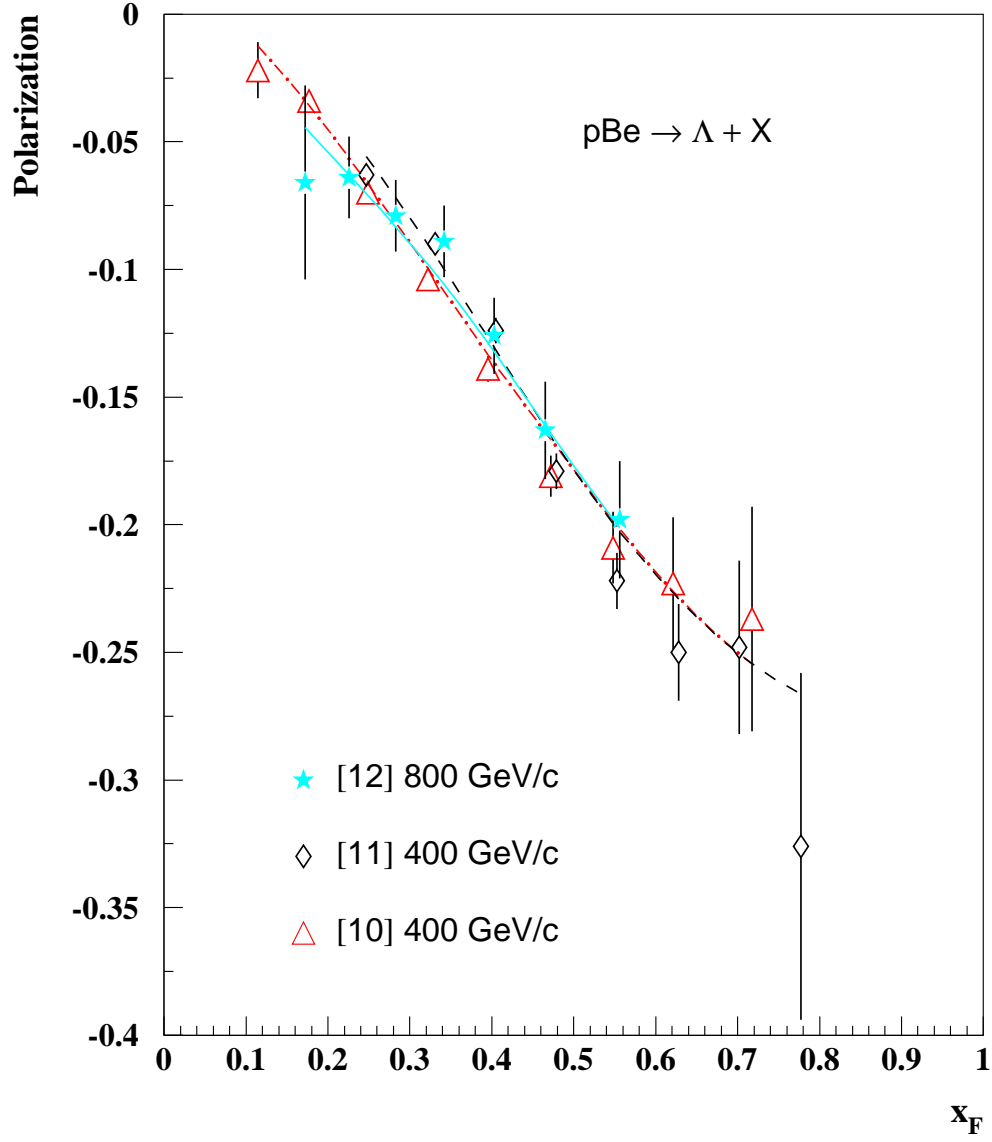


Figure 3: Polarization vs  $x_F$  for  $\Lambda$  production in  $p\text{Be}$  collisions. The fit parameters of eq. (10) are presented in Table 1, fit # 2. The fitting curves correspond to data [12] (solid), [11] (dashed), and [10] (dash-dotted), respectively.

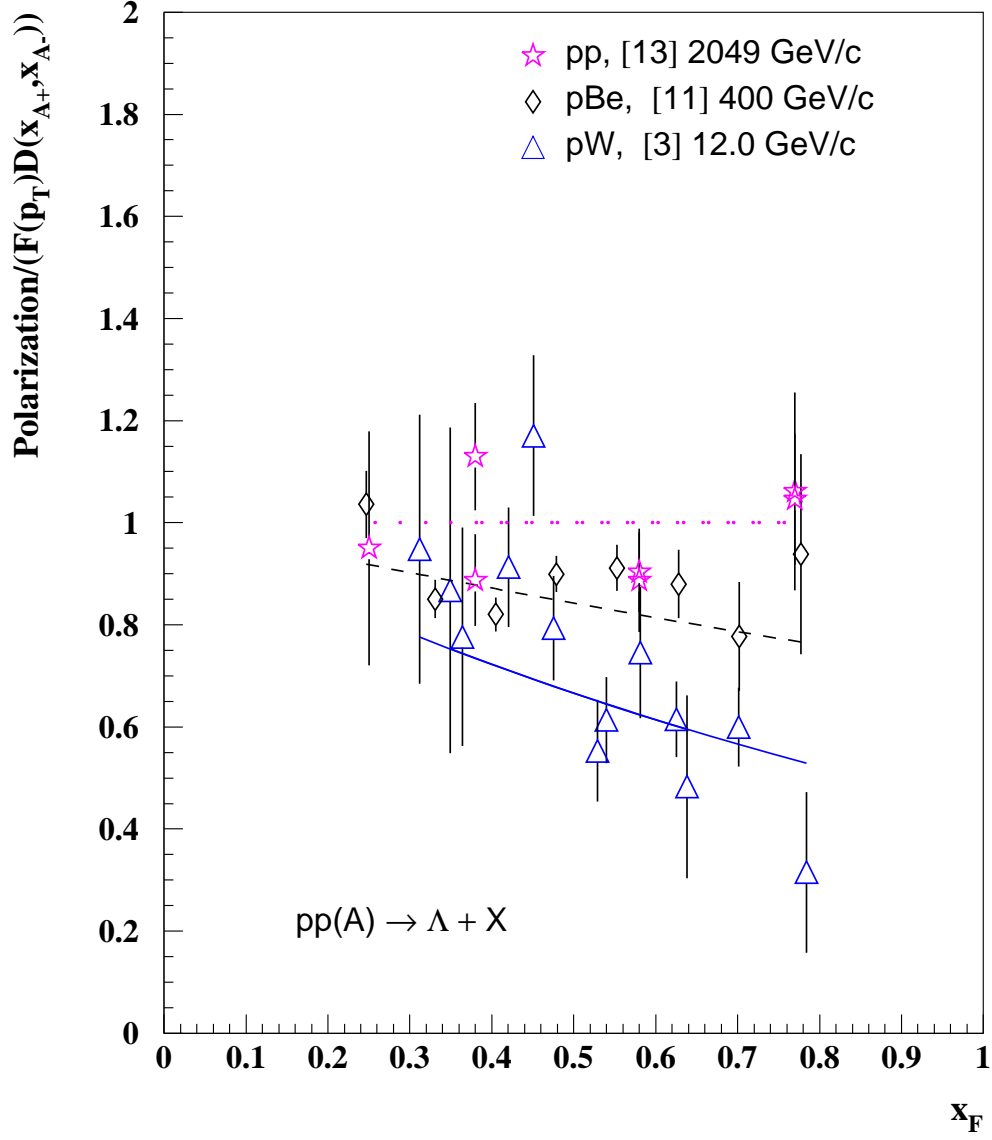


Figure 4: The ratio of polarization and  $F(p_T)D(x_{A+}, x_{A-})$  (see eqs. (10)-(18)) vs  $x_F$  for  $\Lambda$  production in  $pp$  [13],  $pBe$  [11] and  $pW$  [3] collisions. Parameters of eqs. (10)-(15) are presented in Table 1, fit # 2. The curves correspond to the  $pp$  (dotted),  $pBe$  (dashed) and  $pW$  (solid) collisions, respectively.

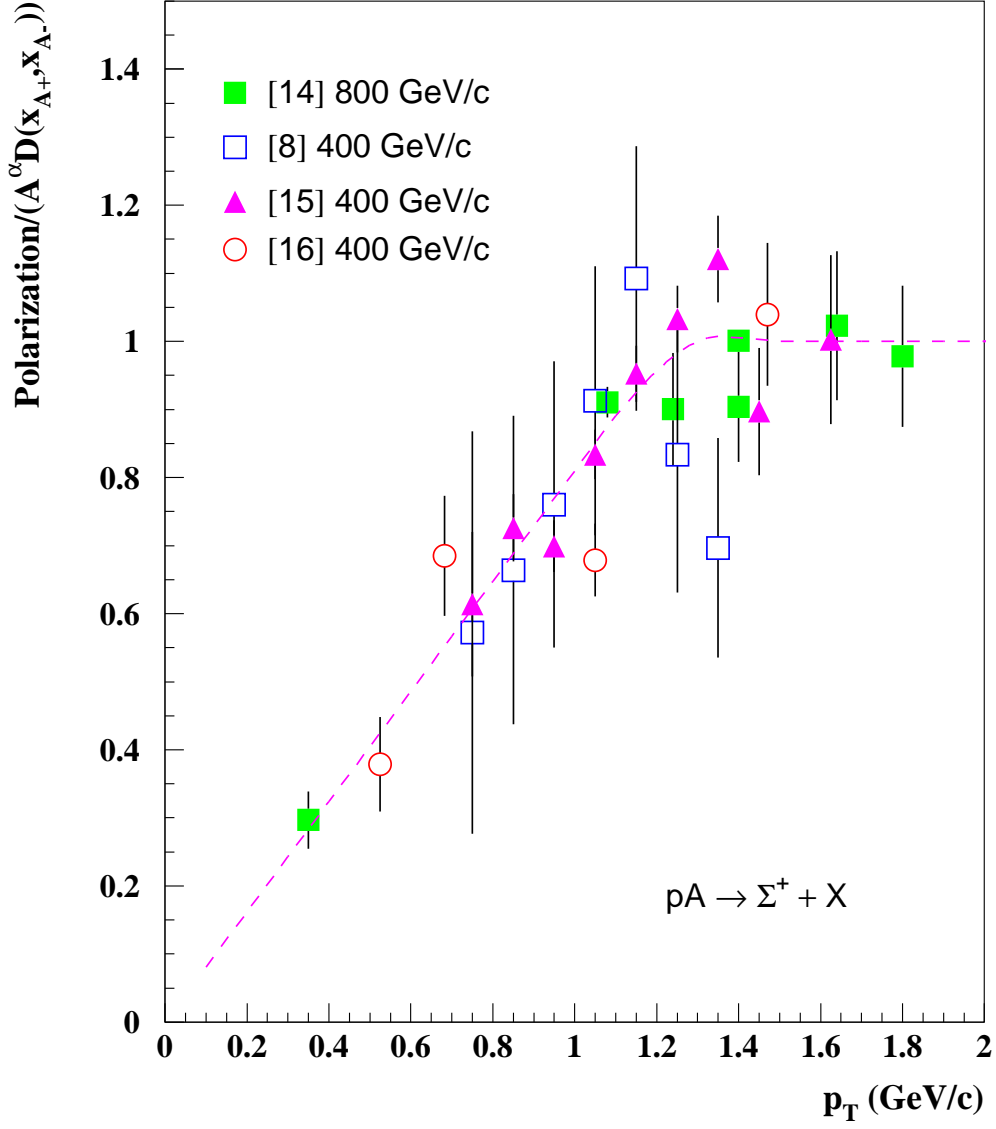


Figure 5: The ratio of polarization and  $A^\alpha D(x_{A+}, x_{A-})$ , (eq. (18)) vs  $p_T$  for  $\Sigma^+$  production in  $pA$  collisions. Parameters of eqs. (11)-(19) are presented in Table 2, fit # 2. The curve corresponds to the function  $F(p_T)$  in eq. (19).

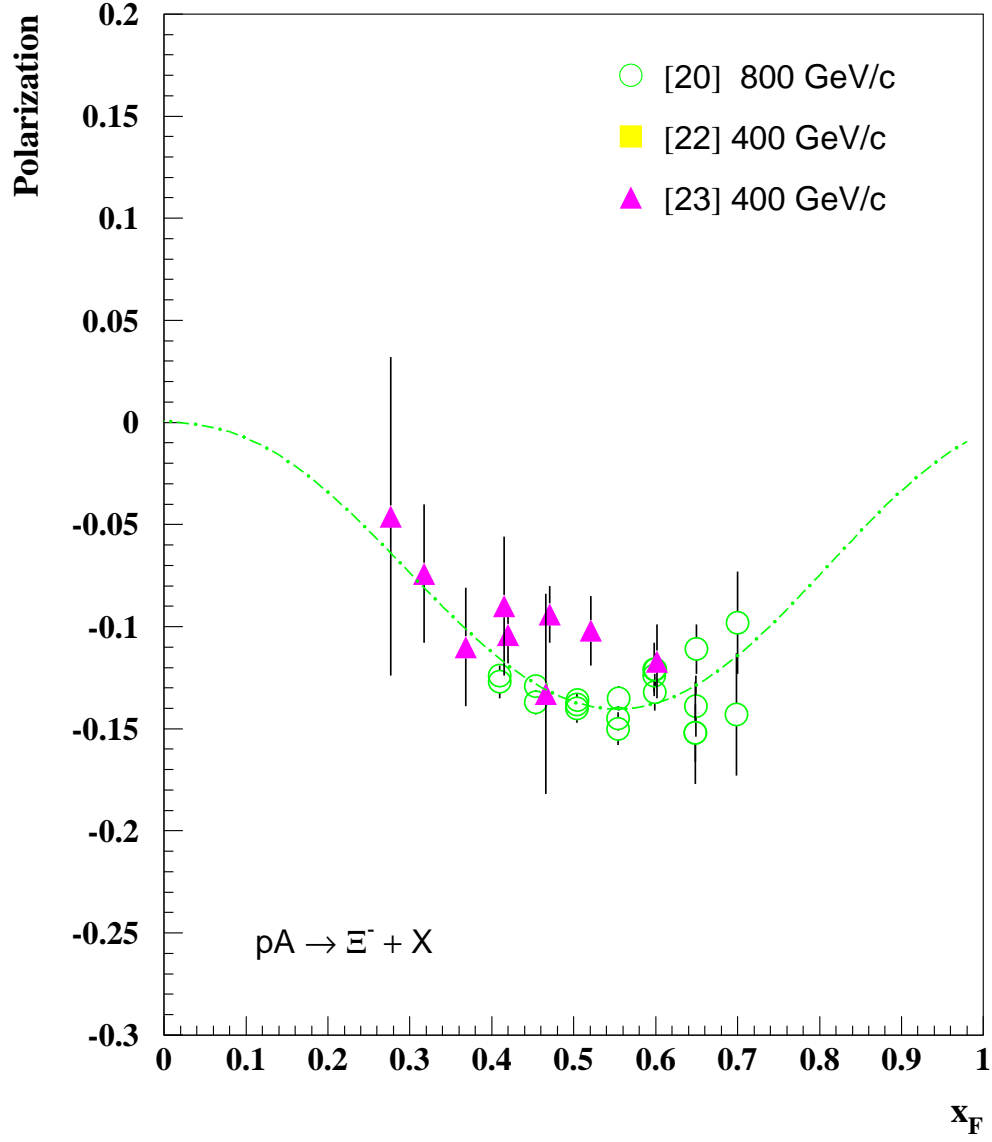


Figure 6: Polarization vs  $x_F$  for  $\Xi^-$  production in  $pA$  collisions. The fit parameters of eqs. (10)-(19) are presented in Table 3. The curve correspond to the fit # 2 for  $p_T = 1.5$  GeV/c.

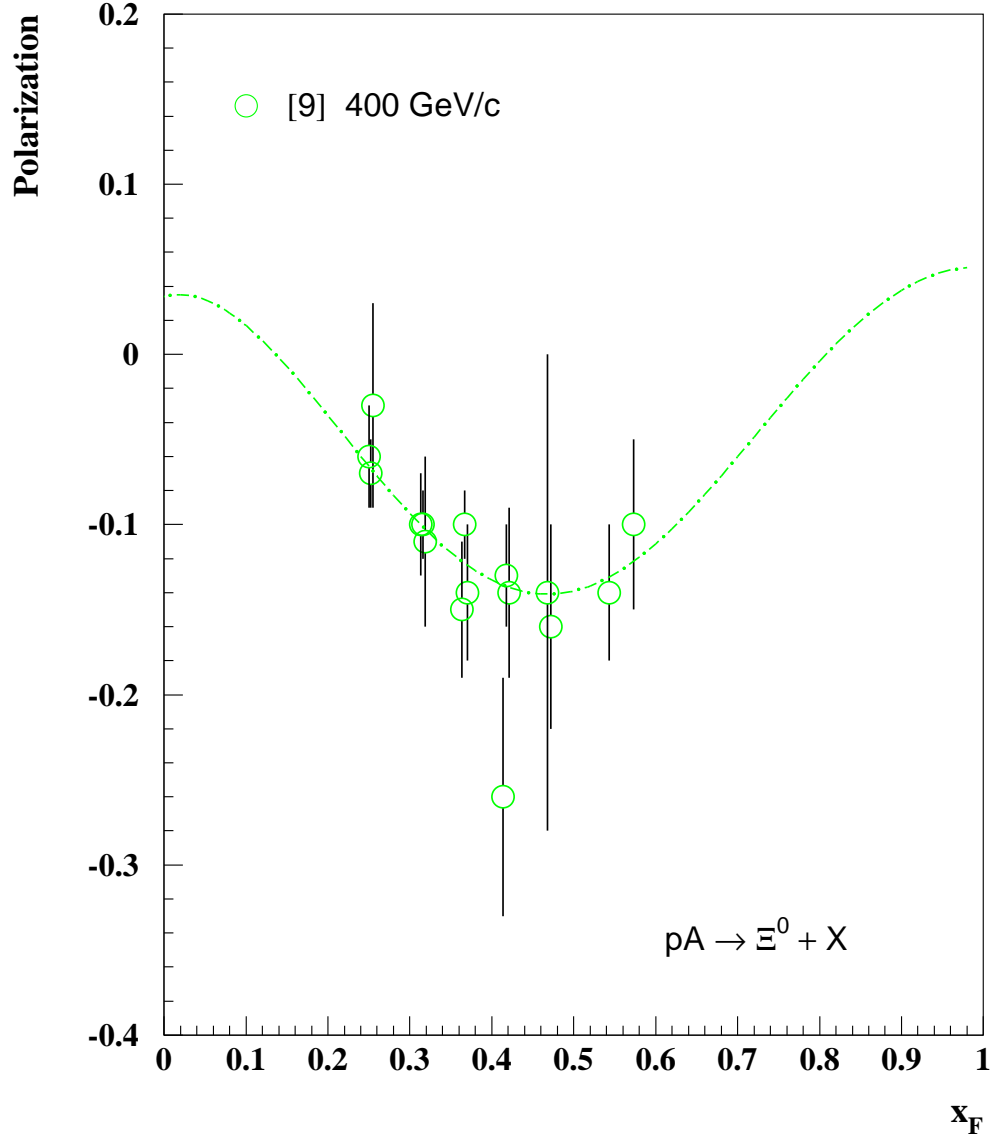


Figure 7: Polarization vs  $x_F$  for  $\Xi^0$  production in  $pA$  collisions. The fit parameters of eqs. (10)-(19) are presented in Table 3. The curve correspond to the fit # 4 for  $p_T = 1.5$  GeV/c.

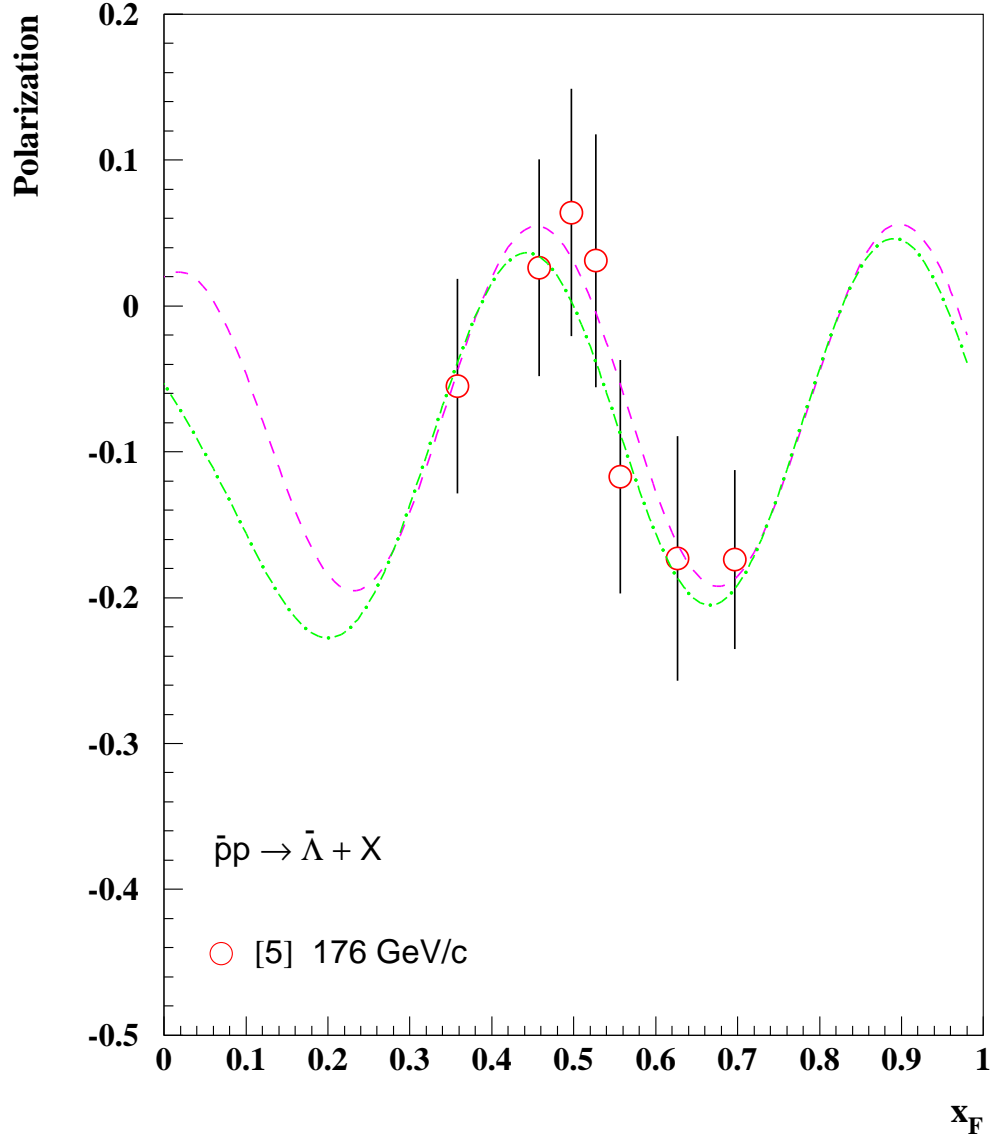


Figure 8: Polarization vs  $x_F$  for  $\bar{\Lambda}$  production in  $\bar{p}p$  collisions. The fit parameters of eqs. (10)-(20) are presented in Table 7. The curves correspond to the fit # 5 for  $p_T = 0.5$  GeV/c (dashed), and  $p_T = 1.5$  GeV/c (dash-dotted), respectively.

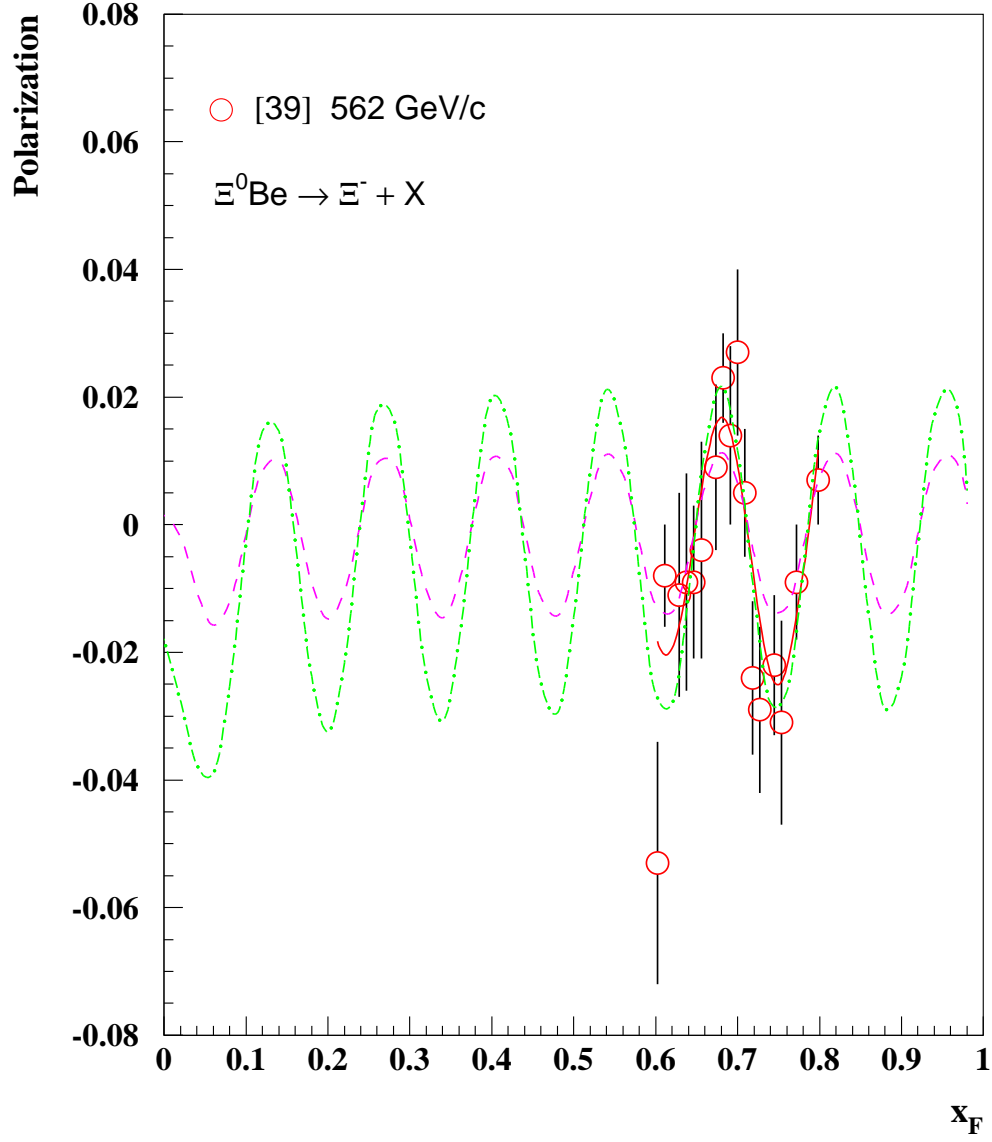


Figure 9: Polarization vs  $x_F$  for  $\Xi^-$  production in  $\Lambda(\Xi^0)p$  collisions. The fit parameters of eqs. (10)-(20) are presented in Table 8. The curves correspond to the fit # 2 for  $p_T = 0.5$  GeV/c (dashed), and  $p_T = 1.5$  GeV/c (dash-dotted), respectively.

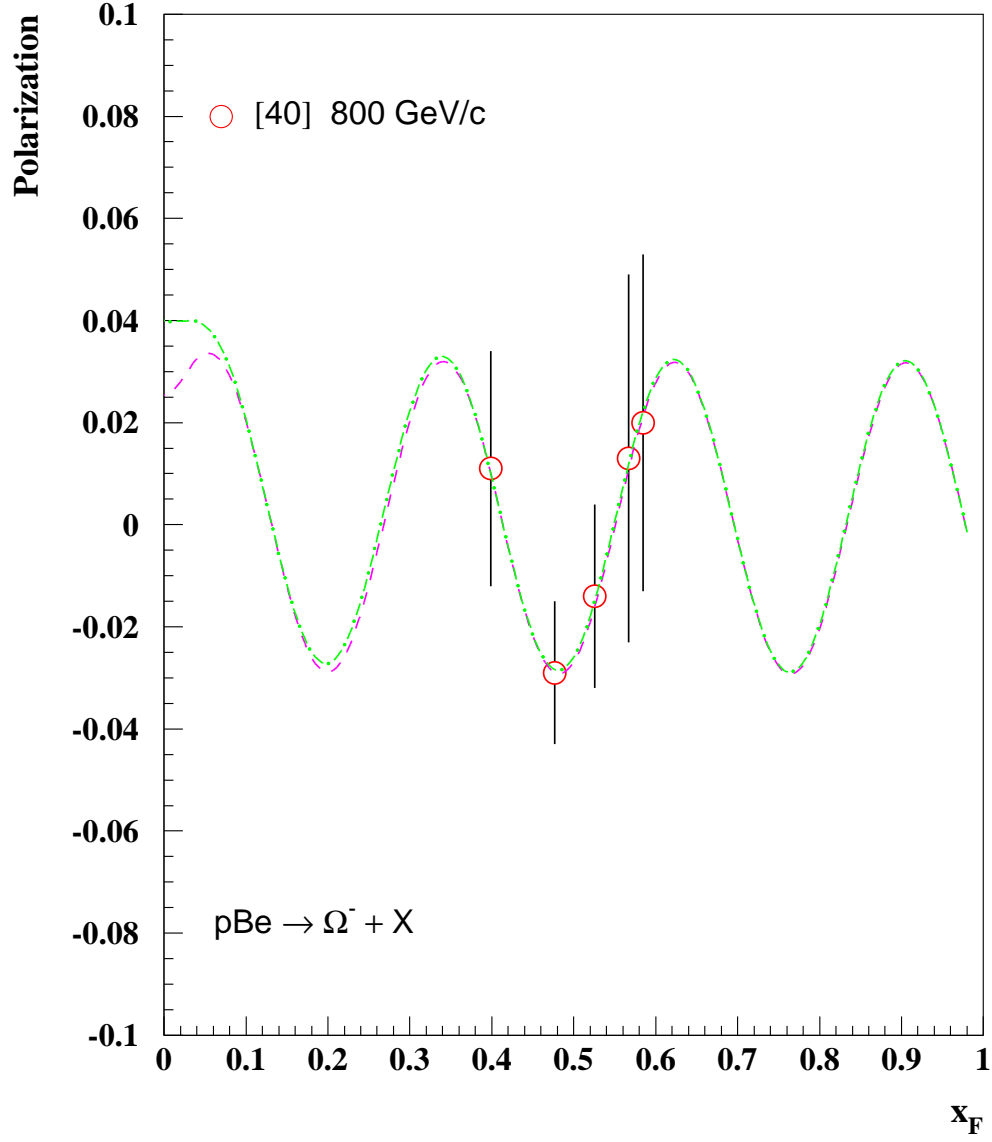


Figure 10: Polarization vs  $x_F$  for  $\Omega^-$  production in  $pBe$  collisions. The fit parameters of eqs. (10)-(19) are presented in Table 8. The curves correspond to the fit # 4 for  $p_T = 0.5$  GeV/c (dashed), and  $p_T = 1.0$  GeV/c (dash-dotted), respectively.



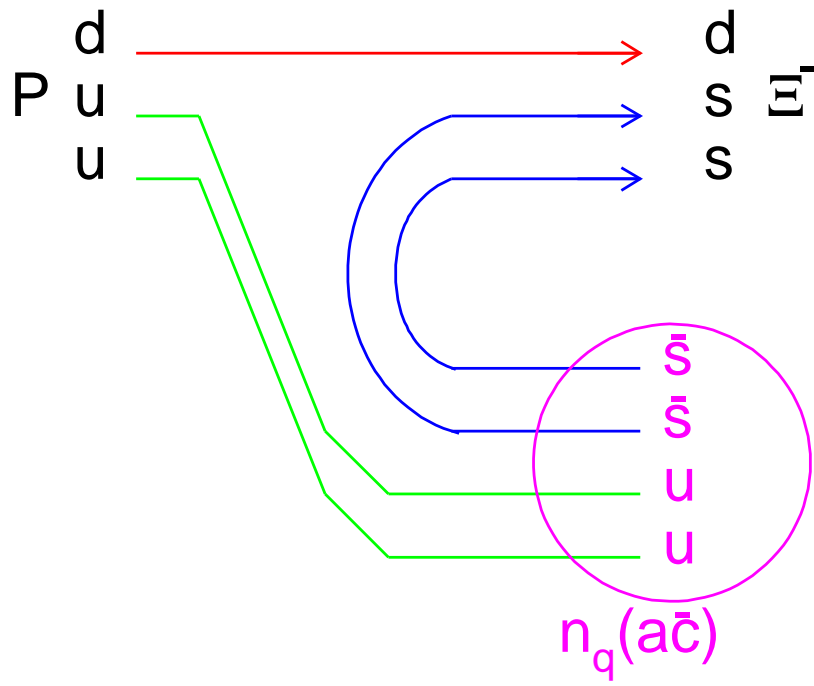


Figure 11: The diagram of a proton fragmentation into a  $\Xi^-$  hyperon. The number of residual quarks is characterized by  $n_q(a\bar{c})$ .

